THE UNIVERSITY OF ALBERTA

AN ANALYSIS OF ELASTOHYDRODYNAMIC LUBRICATION IN LAMINAR FLOW

by

© Kenny K.Y. WONG

A THESIS

SUBMITTED TO THE FACULTY OF GRADUATE STUDIES AND RESEARCH

IN PARTIAL FULFILMENT OF THE REQUIREMENTS FOR THE DEGREE

OF MASTER OF SCIENCE

DEPARTMENT OF MECHANICAL ENGINEERING

EDMONTON, ALBERTA

SPRING 1983

ABSTRACT

An isothermal elastohydrodynamic lubrication of materials of both low and high elastic moduli was being studied. A physical elastohydrodynamic lubrication model for materials of low elastic modulus was postulated. The governing equations for the model are the momentum and continuity equations for fluid and the Hertzian equations for solid. A numerical solution of finding the minimum film thickness of the form $h^{+}_{min}/(U^{+})^{1/2}$ was presented over a wide range of loads, between $w^{+}/(U^{+})^{1/2} = 0.9$ and 20. The results were found to have a good agreement with the earlier experimental results.

A theoretical approach was also used to analyze the elastohydrodynamic lubrication problem under laminar regime. The governing equations for the theoretical analysis are the basic elasticity equation together with the momentum and continuity equations. Results of film thickness and pressure profiles for different h^{+}_{min} were obtained, which were then used to find velocity distribution, load capacity, and drag. The impacts of pressure-dependent viscosity and elastic deformation on the analysis of elastohydrodynamic lubrication were examined. The variations of load and drag with h^{+}_{min} were noted. Present theoretical results were found to have a good agreement with the earlier experimental and theoretical results.

ACKNOWLEDGEMENTS

The author wishes to express deep appreciation to Dr. C.M. Rodkiewicz for his continuing guidance and interest in this study.

Dr. S. Biswas of the Department of Mechanical Engineering, India Institute of Technology, Delhi, India, was associated with this study at the early stage. The author wishes to thank him for his initial guidance and interest.

The author is highly indebted to his fiancee, Fanny, and his family for their unceasing encouragement and understanding during his course of study.

Table of Contents

LIST OF FIGURES

NOMENCLATURE

a = half-Hertzian width = $\sqrt{\frac{4}{\pi}\{\frac{1-\upsilon_1^2}{E_1}+\frac{1-\upsilon_2^2}{E_2}\}wR}$

E = Young's modulus

E_1, E_2 = elastic moduli of solids in contact

$\frac{1}{E'}$ = $\frac{1}{2}(\frac{1-\upsilon_1^2}{E_1}+\frac{1-\upsilon_2^2}{E_2})$

f_1, f_2 = functions defined by Equations(2.21)

F = drag per unit length of cylinder

F_o, F_h = drag per unit length of cylinder at $y=0$ and $y=h$ respectively

G = shear modulus

h = film thickness

h_i = h at x equals +a

h_k = reference film thickness

h_* = h at which pressure is maximum

h_{min} = minimum film thickness

h_o = film thickness at the exit

h_m = minimum separation over the Hertzian contact zone

h_c = central film thickness

L_k = reference width

m = slope of the tilted-pad surface

p = lubricant gage pressure

p_k = reference pressure

p_{max} = maximum film pressure

p_o = maximum Hertzian pressure = $2w/\pi a$

q = reduced pressure

R = radius of the equivalent cylinder
= $R_1R_2/R_1 \pm R_2$

R_1, R_2 = radii of cylinders in contact

Re_k^* = $\frac{u_k L_k \mu}{\rho}\left(\frac{h_k}{L_k}\right)^2$

s = additional coordinate in x-direction

u = velocity in x-direction

u_1, u_2 = surface velocities of the sliding or rolling cylinders

U = $u_1 + u_2$

u_k = reference velocity in x-direction

U = displacement in x-direction

v = velocity in y-direction

v_k = reference velocity in y-direction

V = displacement in y-direction

w = load per unit length of cylinder

W = displacement in z-direction

x, y, z = coordinates

x_0 = value of x at the exit at which $p = dp/dx = 0$

Greek

α = pressure-viscosity coefficient

$\gamma_{xy}, \gamma_{xz}, \gamma_{yz}$ = shear strain components in solids

δ = Hertzian displacement for $|x| > a$

$\epsilon_x, \epsilon_y, \epsilon_z$ = direct strain components in solids

μ = absolute viscosity

μ_0 = absolute viscosity at atmospheric pressure

ν = kinematic viscosity

ρ = density of lubricant

$\sigma_x, \sigma_y, \sigma_z$ = normal stress components
σ_r, σ_θ in solids

τ_0, τ_h = surface shear stresses
at y=0 and y=h respectively

$\tau_{xy}, \tau_{r\theta}$ = shear stress components in solids

υ = Poisson's ratio

υ_1, υ_2 = Poisson's ratio of solids in contact

ϕ = stress function = $(-w/\pi)r\theta\sin\theta$

Dimensionless groups

F^+ = $F/E'R$

g^+ = $\alpha E'$

h^+ = h/R

p^+ = p/E'

q^+ = q/E'

s^+ = s/R

$\bar{s}^+$ = $\bar{s}/R$

u^+ = $u\mu_0/E'R$

V^+ = V/R

w^+ = $w/E'R$

x^+ = x/R

x_s^+ = x/a

y^+ = y/R

δ^+ = δ/R

1. INTRODUCTION

1.1 Statement of the Elastohydrodynamic problem

Elastohydrodynamic lubrication, unlike classical hydrodynamic lubrication, takes into consideration the variation in the viscosity of a lubricant film with pressure and the elastic deformation of the bounding solids. The solution of film shape and pressure profile for a contact thus requires a simultaneous solution of the continuity and momentum equations for the fluid and the elasticity equation for the solid with a viscosity which changes along the film as the pressure varies.

When the bounding solids are made of materials of high elastic modulus ,e.g. metal, elastic deformation is relatively small as compared to the film thickness. High film pressures are generated and cause a large changes in lubricant viscosity along the film. On the other hand for low elastic modulus bounding solids ,e.g. rubber, elastic deformation is relatively large as compared to the film thickness. The film pressures generated between soft contacts are insufficient to cause significant increases in the lubricant viscosity ,in sharp contrast with the metallic case. Therefore, the lubricant in this case may be considered isoviscous.

Though, much attention has been paid to the problems concerning the lubrication of metallic gears, roller bearings and cams, recently there is an increasing interest

in the lubrication of soft elastic surfaces which finds itself important in the lubrication of, for instance, reciprocating seals, flexible-pad thrust bearings and motor car tyres aquaplaning on wet roads.

In the present study, analysis will be made under laminar regime for both high and low elastic moduli bounding solids under isothermal elastohydrodynamic lubrication condition.

The geometry of the bounding solids are chosen as two rotating elastic cylinders with a thin lubricant film in between. This particular geometry is chosen because of the fact that many contacts between machine components can be represented by cylinders which provide good geometrical agreement with the profile of the undeformed solids in the immediate vicinity of the contact.

In summary, results obtained from the present study are
(i) film profiles.
(ii) pressure profiles from which load capacity can be obtained.
(iii) velocity profiles from which drag force can be computed.

1.2 Review of relevant literature

The early interest in the subject of elastohydrodynamic lubrication arose from the study of gear lubrication. Martin [1] approached the gear lubrication problem by considering the equivalent problem of the lubrication of a cylinder near

a plane with the assumptions that the lubricating contacts were rigid and lubricant was isoviscous and incompressible. From his work, three useful relations were obtained.

$$x_0^+=-0.672(h_{min}^+)^{1/2} \tag{1.1a}$$

$$p_{max}^+=1.074\frac{U^+}{(h_{min}^+)^{1.5}} \tag{1.1b}$$

$$w^+=2.448\frac{U^+}{h_{min}^+} \tag{1.1c}$$

However, film thickness predicted by his theory could not account for the existence of fluid films which were thick enough to prevent severe metallic contact in gears.

In the early 1960's, gears lubricated by a hydrodynamic action was confirmed by direct film thickness measurements in disc machine designed to simulate gear tooth contact. Crook [2], using a capacitance technique, measured the film thickness which was of the order of $2x10^{-4}$mm (10^{-5} inches).

Peppler [3] and Meldahl [4] examined the effect of elastic deformation in the gear lubrication problem. Neither Peppler's nor Meldahl's work suggested that elastic deformation alone could be responsible for the existence of a continuous fluid film between gear teeth.

Gatcombe [5] examined the influence of high pressure upon lubricant viscosity. His work suggested that the effect of the viscosity-pressure characteristics of a lubricant alone could not account for the existence of a continuous fluid film in gear contacts.

Grubin [6] developed an approximate film thickness formular which included the effect of elastic distortion and pressure dependent viscosity. He assumed that the elastic distortion would take the form of Hertzian deformation under highly loaded conditions. His predicted values of the film thickness were orders of magnitude greater than that of the Martin's, and consistent with the formation of a continuous fluid film between gear teeth. One useful relation emanating from his work in terms of dimensionless quantities is

$$h_m^+=1.176(g^+U^+)^{8/11}/(w^+)^{1/11} \tag{1.2}$$

However, the exact features of the contact mechanism do not emerge from this simple analysis.

Dowson and Whitaker [7] presented a solution to the problem of elastohydrodynamic lubrication of highly loaded elastic cylinders with the variation of viscosity with pressure under isothermal condition. A numerical method is developed which enables a pressure curve to be found which satisfies the elastic and hydrodynamic compatibility of the system. However their method suffers from the fact that adjustment of the pressures during iteration has to be done manually and required experienced guessing, and that it is only applicable for very heavily loaded contacts. One useful relation obtaining from this work in terms of dimensionless quantities is

$$h_{min}^+=0.985(g^+)^{0.6}(U^+)^{0.7}/(w^+)^{0.13} \tag{1.3}$$

Osterle and Stephenson [8] obtained elastohydrodynamic solution for 'hard' materials by a direct approach. His

analysis included not only the effect of pressure-dependent viscosity and elastic distortion but also the effect of compressibility of the lubricant. However, no results were obtained for 'soft' elastic materials.

Herrebrugh [9] showed that the hydrodynamic and elasticity equations in elastohydrodynamic lubrication can be combined into one single integral equation. A numerical solution of this integral equation for constant viscosity was presented. However, the resulting solutions were only claimed to be approximate.

Cheng [10] presented the isothermal elastohydrodynamic theory for the full range of pressure-viscosity parameter,g^+. His work suggested that for small values of g^+, the lubricant could be treated as isoviscous fluid.

In the late 1960's, increasing interest was given to the elastohydrodynamic problem lubrication for materials of low elastic modulus. Roberts and Tabor [11] employed an interferometric technique to study the fluid film lubrication of rubber. He showed that the deformed shape of rubber surface took the shape of a tilted pad surface along most of the contact region.

Higginson [12] presented a model experiment in elastohydrodynamic lubrication of rubber. From his pressure measurements, he found the development of a near-Hertzian pressure curve as load increased.

Roberts and Swales [13] studied the elastohydrodynamic lubrication of a rubber cylinder sliding over a glass plate

using an optical interference technique. They also used an iterative process similar to [7] to solve the basic lubrication and elastic equations simultaneously and obtained solutions mainly for lightly loaded contacts. They found the discrepancy between theory and experiment at light loads and high speeds, this might be accounted for by side-leakage effects.

Baglin and Archard [14] presented an analytic solution of this problem, which was similar to the type of Grubin theory except they used simplied Hertzian displacement equation. In addition, they required to find a criterion for the pressure at the inlet edge of a nearly Hertzian region to ensure that the necessary distribution of pressure was generated within the Hertzian zone. Their results of the minimum film thickness had to be modified by a factor of 0.8, in order to provide a comparison with the earlier computer solutions [9].

Swales, Dowson and Latham [15] described a comprehensive experimental and theoretical treatment of the lubrication of soft elastic materials. The effect of inlet starvation on oil film thickness was also investigated. The experimental study involved a sliding contact between a rubber cylinder and a smooth plane. Pressure and film thickness profiles were measured at the same time, using piezoelectic and capacitance transducers respectively. The theoretical work was similar to that described on detail elsewhere [7], except the lubricant was assumed to be

isoviscous. Again the method suffers the same difficulties as stated previously. In addition, they found that it was difficult to achieve solutions for the case of large surface displacements. They were unable to decide whether the reason for the instability lay with the equations or with the computing methods. In general, they found both the experimental and theoretical results were comparable.

1.3 Equivalent cylinders

In the present study, a film of relatively short width will be considered between the contacts. Therefore the undeformed solids can be sufficiently represented by two cylinders in the region of the contact zone. These two cylinders can further be represented by a geometrically equivalent cylinder near a rigid plane as shown in Fig(1). The geometrical requirement is that the gap between the cylinders in the original and equivalent contact should be the same at equal values of x.

If the centres of the two cylinders lie on the same side of the common tangent at the contact point then the radius of the equivalent cylinder takes the form of

$$\frac{1}{R} = \frac{1}{R_2} - \frac{1}{R_1} \quad \text{where } R_1 > R_2$$

Force components on the initial and equivalent systems shown in Fig(1) can be related as follows:

For hydrodynamic force in vertical direction:

$$w_{y1} = w_{y2} = w_y = \int p \, dx \tag{1.5}$$

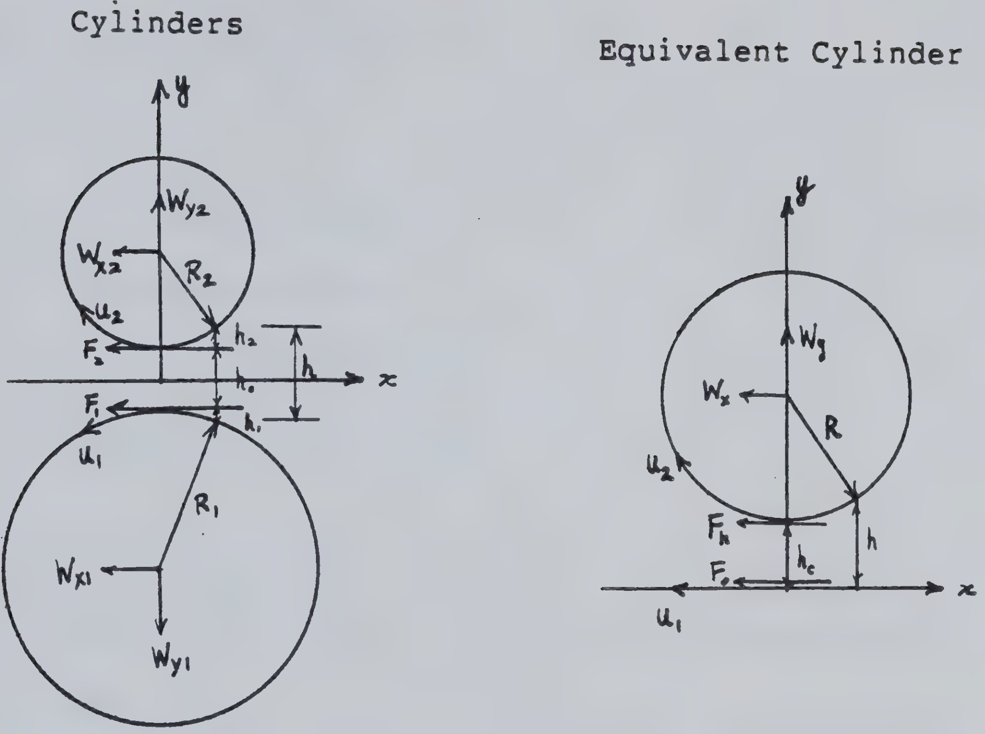

(a) (b)

$$h_1=R_1-\sqrt{R_1^2-x^2} \cong x^2/2R_1$$

Similarly

$$h_2 \cong x^2/2R_2$$

Hence

$$\begin{aligned} h&=h_c+h_1+h_2 \\ &\cong h_c+(x^2/2)\ (1/R_1+1/R_2) \\ &=h_c+x^2/2R \end{aligned} \tag{1.4}$$

where $1/R=1/R_1+1/R_2$

Fig(1) Representation of a contact between two cylinders by an equivalent cylinder near a plane

For hydrodynamic force in horizontal direction:

$$w_{x1}=-\int p\ dh_1=-(\int px\ dx)/R_1 \qquad (1.6a)$$

$$w_{x2}=-\int p\ dh_2=-(\int px\ dx)/R_2 \qquad (1.6b)$$

$$w_x=-\int p\ dh=-(\int px\ dx)/R \qquad (1.6c)$$

Hence

$$w_{x1}=(R/R_1)w_x \text{ and } w_{x2}=(R/R_2)w_x \qquad (1.6d,e)$$

For drag force components:

$$F_2=F_h=\int \tau_h\ dx=\int \mu(\partial u/\partial y)|_{y=h}\ dx \qquad (1.7a)$$

$$F_1=F_0=\int \tau_0\ dx=\int \mu(\partial u/\partial y)|_{y=0}\ dx \qquad (1.7b)$$

1.4 General assumptions

The assumptions which will be made in the analysis are stated below :

(1) The cylinders are infinitely long i.e. side leakage is neglected and flow becomes two dimensional.

(2) All inertia effects are neglected.

(3) The width of the contact region is much smaller than the radii of the cylinders.

(4) The film thickness is much smaller than the width of the contact.

(5) The flow is in steady state.

(6) The lubricant is incompressible.

(7) There is no slip at the boundaries.

(8) The solids will be treated as perfectly elastic and in a condition of plane strain.

(9) The contact will be represented by an equivalent cylinder near a plane.

2. PHYSICAL MODELLING APPROACH IN SOFT CONTACT

2.1 Description of the elastohydrodynamic model

A physical elastohydrodynamic lubrication model as shown in Fig(2) is postulated from which a numerical solution of finding the minimum film thickness is presented under isothermal condition. The theory of elastohydrodynamic lubrication of high elastic modulus materials was not developed until Grubin [6] included the effect of elastic distortion of the bounding solids and the pressure-dependent viscosity of the lubricant. However, little attention has been paid to the development of the theory for soft materials in which deformation rather than pressure-viscosity effect becomes dominant. The lubricant in such case can be regarded as isoviscous fluid as suggested by Cheng [10].

Since there is no significant increase in pressure due to pressure-viscosity effect in the case of soft contacts, the generated pressure of the lubricant must be entirely due to hydrodynamic action, i.e., a converging bearing configuration must exist along the pressure zone. In the light of this configuration and the interferometric study done by Roberts and Tabor [11], it is postulated that the deformed cylinder under elastohydrodynamic lubrication will have a shape like tilted-pad surface of finite slope along most of the contact region as shown in Fig(2a).

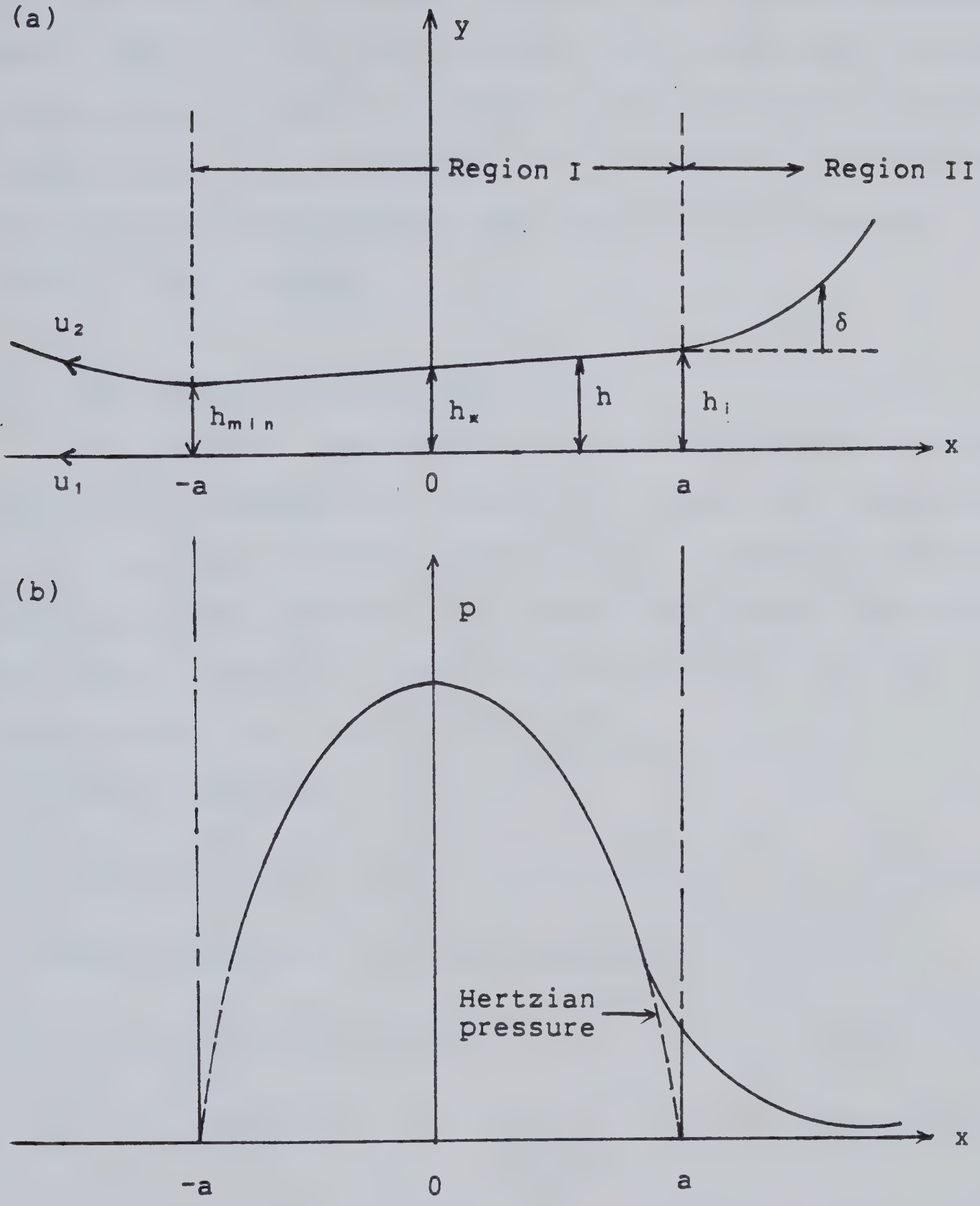

Fig(2) Geometry of lubrication film and model pressure distribution

Furthermore, from the film pressure measurements done by Higginson [12], pressure profiles for increasing load were found to be very close to that of Hertzian pressure distribution as shown in Fig(2b). In the light of this experiment, it is postulated that the deformed shape of the cylinder outside the tilted pad region will be the same as that in a dry contact.

2.2 General equations for fluid

The general equations governing the steady, laminar flow of an incompressible lubricant through an infinitely long rotating cylinder and a plane slider, as shown in Fig(2), are the momentum equations in the x and y directions and the continuity equation. The general form of the equations may be listed as follows:

x-momentum equation

$$u\frac{\partial u}{\partial x}+v\frac{\partial u}{\partial y}=-\frac{1}{\rho}\frac{\partial p}{\partial x}+\nu\left(\frac{\partial^2 u}{\partial x^2}+\frac{\partial^2 u}{\partial y^2}\right) \qquad (2.1)$$

y-momentum equation with body force neglected

$$u\frac{\partial v}{\partial x}+v\frac{\partial v}{\partial y}=-\frac{1}{\rho}\frac{\partial p}{\partial y}+\nu\left(\frac{\partial^2 v}{\partial x^2}+\frac{\partial^2 v}{\partial y^2}\right) \qquad (2.2)$$

Continuity equation

$$\frac{\partial u}{\partial x}+\frac{\partial v}{\partial y}=0 \qquad (2.3)$$

In all the later analysis, the following velocity boundary conditions will be adopted.

$y=0$: $u=-u_1, v=0$ (2.4a,b)

$y=h$: $u=-u_2, v\cong -u_2(\partial h/\partial x)$ (2.4c,d)

Particularly for the presently discussed model, the following pressure boundary conditions will be adopted.

$x=+\infty$: $p=0$ (2.5a)

$x=-a$: $p=0$ (2.5b)

$x=0$: $p=p_{max}=p_o$ and $\frac{dp}{dx}=0$ (2.5c,d)

2.3 Specialized equation for lubrication

For representative lubricating films, the inertia forces can be shown to be negligible compared with the viscous force by the following order of magnitude analysis.

Selecting appropriate reference quantities, the variables can be expressed as follows:

$x=\bar{x}L_k$

$y=\bar{y}h_k$

$u=\bar{u}u_k$

$v=\bar{v}v_k$

$p=\bar{p}p_k$

Now substituting all the transformed variables into the governing Equations(2.1) to (2.3), and comparing the relative magnitude of the viscous terms with the inertia terms in each of the momentum equations, we obtain

For continuity equation

$$\frac{\partial \bar{u}}{\partial \bar{x}}+\left(\frac{v_k L_k}{u_k h_k}\right)\frac{\partial \bar{v}}{\partial \bar{y}}=0$$

It is noted that, $\partial\bar{u}/\partial\bar{x}$ and $\partial\bar{v}/\partial\bar{y}$ are of order 1. Consequently, the term $v_k L_k/u_k h_k$ must be of order 1. Choosing $v_k L_k/u_k h_k=1$, we can write $v_k= u_k(h_k/L_k)$ which will be used in the order of magnitude analysis for the momentum equations.

For the x-momentum equation

$$\bar{u}\frac{\partial\bar{u}}{\partial\bar{x}}+\bar{v}\frac{\partial\bar{u}}{\partial\bar{y}}=-\frac{p_k}{\rho u_k^2}\frac{\partial\bar{p}}{\partial\bar{x}}+\frac{1}{Re_k^*}\left[\left(\frac{h_k}{L_k}\right)^2\frac{\partial^2\bar{u}}{\partial\bar{x}^2}+\frac{\partial^2\bar{u}}{\partial\bar{y}^2}\right]$$

Since the lubricating film is very thin as compared to the width of the contact region, i.e. $h_k/L_k<<1$, therefore the viscous term $\partial^2 u/\partial x^2$ is negligibly small compared to $\partial^2 u/\partial y^2$. If $Re_k^*<<1$, then the inertia terms can be neglected compared to viscous term. Hence only pressure and viscous forces will be present. Consequently Equation(2.1) reduces to

$$\frac{\partial p}{\partial x}=\mu\frac{\partial^2 u}{\partial y^2} \tag{2.6}$$

In fact, Re_k^* is much less than one in most lubrication situations.

For the y-momentum equation:

$$\bar{u}\frac{\partial\bar{v}}{\partial\bar{x}}+\bar{v}\frac{\partial\bar{v}}{\partial\bar{y}}=-\left(\frac{L_k}{h_k}\right)^2\frac{p_k}{\rho u_k^2}\frac{\partial\bar{p}}{\partial\bar{y}}+\frac{1}{Re_k^*}\left[\left(\frac{h_k}{L_k}\right)^2\frac{\partial^2\bar{v}}{\partial\bar{x}^2}+\frac{\partial^2\bar{v}}{\partial\bar{y}^2}\right]$$

Since $h_k/L_k<<1$, therefore $\partial^2 v/\partial y^2>>\partial^2 v/\partial x^2$; and if $Re_k^*<<1$, inertia terms can be neglected as compared to viscous term. Consequently Equation(2.2) reduces to

$$\frac{\partial p}{\partial y}=\mu\frac{\partial^2 v}{\partial y^2} \tag{2.7}$$

Now comparing the terms on the right hand side of Equations(2.6) and (2.7), we have

From Equation(2.6)

$$\frac{\partial p}{\partial x}=(\mu\frac{u_k}{h_k^2})\frac{\partial^2\bar{u}}{\partial\bar{y}^2}$$

From Equation(2.7)

$$\frac{\partial p}{\partial y}=\frac{h_k}{L_k}(\mu\frac{u_k}{h_k^2})\frac{\partial^2\bar{v}}{\partial\bar{y}^2}$$

It is noted that $\partial p/\partial y$ is (h_k/L_k) times the order of magnitude of $\partial p/\partial x$. Since $h_k/L_k<<1$, the variation of pressure across the lubricant film is quite insignificant. Therefore the momentum equation for the y-direction can be omitted altogether. Thus write, $\partial p/\partial x\cong dp/dx$.

Now the reduced set of equations only includes x-momentum equation and continuity equation of the following forms.

x-momentum equation:

$$\frac{dp}{dx}=\mu\frac{\partial^2 u}{\partial y^2} \qquad (2.8)$$

Continuity equation:

$$\frac{\partial u}{\partial x}+\frac{\partial v}{\partial y}=0 \qquad (2.9)$$

Furthermore, Equations(2.8) and (2.9) can be combined into one single equation as described below.

Integrating Equation(2.8) twice with respect to y, yields

$$u=\frac{1}{\mu}\frac{dp}{dx}\frac{y^2}{2}+c_1y+c_2$$

Applying boundary conditions(2.4a,c), leads to

$$c_1=\frac{1}{h}(u_1-u_2)-\frac{1}{\mu}\frac{dp}{dx}\frac{h}{2} \quad \text{and} \quad c_2=-u_1$$

Hence the velocity distribution is

$$u=\frac{1}{\mu}\frac{dp}{dx}\left[\frac{y^2}{2}-\frac{hy}{2}\right]+\frac{y}{h}(u_1-u_2)-u_1 \tag{2.10}$$

Integrating Equation(2.9) with respect to y, leads to

$$\frac{\partial}{\partial x}\int_0^h u\,dy-(-u_2)\frac{\partial h}{\partial x}+[v]_0^h=0$$

Applying boundary conditions(2.4b,d) the second and third terms of the above equation will cancel each other out. Substituting the expression for u in Equation(2.10) into the above equation, and then carrying the integration, leads to

$$\frac{d}{dx}\left[\frac{1}{\mu}\frac{dp}{dx}\frac{h^3}{12}\right]=-\frac{U}{2}\frac{dh}{dx} \tag{2.11}$$

which is the famous Reynolds equation.

Upon integrating Equation(2.11) with respect to x, leads to

$$\frac{1}{\mu}\frac{dp}{dx}\frac{h^3}{12}=-\frac{U}{2}h+c_3$$

Now applying boundary condition(2.5d), leads to

$$c_3=\frac{Uh_*}{2}$$

where h_* is defined as the film thickness at which pressure is maximum. Hence

$$\frac{dp}{dx}=-6\mu U\left(\frac{h-h_*}{h^3}\right) \tag{2.12}$$

2.4 Film thickness equation with Hertzian relations

In region I, as shown in Fig(2a), the film thickness variation is linear with x and of slope m. It takes the form

$$h=h_{min}+m(x+a) \tag{2.13}$$

Hence

$$h_{*}=h_{min}+ma \tag{2.14}$$

In region II, the film thickness will take the shape of Hertzian displacement.

$$h=h_{i}+\delta$$

But from Equation(2.13)

$$h_{i}=h_{min}+2ma$$

Therefore

$$h=h_{min}+2ma+\delta \tag{2.15}$$

From Hertzian relations[16]

$$\delta\equiv\left(\frac{1-\upsilon_1^2}{E_1}+\frac{1-\upsilon_2^2}{E_2}\right)ap_0\left\{\left|\frac{x}{a}\left(\frac{x^2}{a^2}-1\right)^{1/2}-\ln\left|\left[\frac{x}{a}+\left(\frac{x^2}{a^2}-1\right)^{1/2}\right]\right|\right|\right\} \tag{2.16a}$$

$$a=\left(\frac{4}{\pi}\left[\frac{1-\upsilon_1^2}{E_1}+\frac{1-\upsilon_2^2}{E_2}\right]wR\right)^{1/2} \tag{2.16b}$$

$$p_0=\frac{2w}{\pi a} \tag{2.16c}$$

2.5 Non-dimensional procedure

Using the Hertzian relations in Equations(2.16), the Equations(2.12), (2.13) and (2.15) can be non-dimensionalized by introducing the following dimensionless variables.

$$x_s^+=\frac{x}{a}\ ,\ h^+=\frac{h}{R}\ ,\ \delta^+=\frac{\delta}{R}\ ,\ p^+=\frac{p}{E'}\ ,\ U^+=\frac{U\mu}{E'R}\ ,\ w^+=\frac{w}{E'R}$$

Equation(2.12) is non-dimensionalized to

$$\frac{dp^+}{dx_s^+}=-6U^+\left(\frac{8w^+}{\pi}\right)^{1/2}\left(\frac{h^+-h_*^+}{h^{+3}}\right) \tag{2.17a}$$

Substituting the dimensionless form of Equation(2.14) into the above equation, yields

$$\frac{dp^+}{dx_s^+}=-6U^+\left(\frac{8w^+}{\pi}\right)^{1/2}\left(\frac{h^+-h_{min}^+-m(8w^+/\pi)^{1/2}}{h^{+3}}\right) \tag{2.17b}$$

Equation(2.13) representing film thickness in region I is non-dimensionalized to

$$h^+=h_{min}^++m\left(\frac{8w^+}{\pi}\right)^{1/2}(1+x_s^+)\ ,\qquad (-1\le x_s^+\le 1) \tag{2.18}$$

Equation(2.15) representing film thickness in region II is non-dimensionalized to

$$h^+=h_{min}^++2m\left(\frac{8w^+}{\pi}\right)^{1/2}+\delta^+\ ,\qquad (x_s^+\ge 1) \tag{2.19}$$

where

$$\delta^+=\frac{4}{\pi}w^+\{|x_s^+(x_s^{+2}-1)^{1/2}-\ln|[x_s^++(x_s^{+2}-1)^{1/2}]||\}$$

The corresponding non-dimensional boundary conditions become

$$x_s^+=+\infty\ :\ p^+=0 \tag{2.20a}$$

$$x_s^+=-1\ :\ p^+=0 \tag{2.20b}$$

$$x_s^+=0\ :\ p^+=p^+_{max}=p_0^+ \tag{2.20c}$$

2.6 Numerical analysis

In this section numerical methods will be described for the solutions of h^+_{min} and m through the pressure equation(2.17b), subject to the boundary conditions(2.20), where the film thickness is given by Equations(2.18) and (2.19) in regions I and II, respectively. Input parameters U^+ and w^+ must be given to define a particular problem.

Initially, the pressure equation is solved in the first half of region I by first assuming h^+_{min} and m, and applying boundary conditions(2.20b) at $x^+_s=-1$. The pressure equation is then integrated, using Simpson's rule, in the positive x^+_s-direction and boundary condition(2.20c) is checked. If it is not satisfied, a new value of h^+_{min} is tried, but with m remaining constant, until the boundary condition(2.20c) is satisfied. Then with these values of new h^+_{min} and m, the pressure equation(2.17b) is again integrated in the positive x-direction between $x^+_s=-1$ and $x^+_s=+\infty$, and boundary condition(2.20a) is checked. If it is not satisfied, a new value of m is tried. The whole process is repeated until the assumed values of h^+_{min} and m satisfy all the boundary conditions(2.20).

In actual numerical procedure, it is assumed that $p^+=0$ at $x^+_s=+\infty$ reaches its asymptotic value when the magnitudes of the pressure and pressure gradient become less than a specified fraction (10^{-3}) of the maximum pressure and maximum pressure gradient, respectively. Also the relative error allowance on matching $p^+(max)=p^+_0$ at $x^+_s=0$ is specified

to be less than 10^{-3}.

A Newton Raphson iterative technique is employed to converge h^+_{min} and m on the solutions. This technique, which is quadratically convergent, can be used because of the fact that a pair of nonlinear equations can be set up as the functions of two variables, h^+_{min} and m. Basically, this pair of nonlinear equations is derived from the boundary conditions(2.20) and is of the following form

$$f_1(h^+_{min},m)=\int_{x_s^+=-1}^{x_s^+=0}\left[\left.\frac{dp^+}{dx_s^+}\right|_{I}\right] dx_s^+ - p_0^+ \qquad (2.21a)$$

and

$$f_2(h^+_{min},m)=\int_{x_s^+=-1}^{x_s^+=1}\left[\left.\frac{dp^+}{dx_s^+}\right|_{I}\right]dx_s^+ + \int_{x_s^+=1}^{x_s^+=+\infty}\left[\left.\frac{dp^+}{dx_s^+}\right|_{II}\right]dx_s^+ \qquad (2.21b)$$

It is noted that in order to satisfy all the boundary conditions(2.20), the assumed values of h^+_{min} and m must be the roots of the functions f_1 and f_2,

i.e. $f_1(h^+_{min},m)=f_2(h^+_{min},m)=0$.

The roots are found by Newton Raphson iterative method as described below:

$$\begin{bmatrix} m \\ \\ h^+_{min} \end{bmatrix}_{t+1} = \begin{bmatrix} m \\ \\ h^+_{min} \end{bmatrix}_{t} - \begin{bmatrix} \dfrac{\partial f_1}{\partial m} & \dfrac{\partial f_1}{\partial h^+_{min}} \\ \dfrac{\partial f_2}{\partial m} & \dfrac{\partial f_2}{\partial h^+_{min}} \end{bmatrix}_{t}^{-1} \begin{bmatrix} f_1 \\ \\ f_2 \end{bmatrix}_{t}$$

All the partial derivatives are approximated by making a small change in the value of a variable and dividing the change in value of the function by the change in value of the variable. Mathematically, it takes the form

$$\frac{\partial f_{1,2}}{\partial m} \cong \frac{f_{1,2}(m+\Delta, h^{+}_{min}) - f_{1,2}(m, h^{+}_{min})}{\Delta}$$

$$\frac{\partial f_{1,2}}{\partial h^{+}_{min}} \cong \frac{f_{1,2}(m, h^{+}_{min}+\Delta) - f_{1,2}(m, h^{+}_{min})}{\Delta}$$

The subscript t indicates the number of the iteration. The iterations are carried out until the difference between two consecutive sets of values is less than a specified relative error allowance (10^{-3}).

A criterion for convergence of Newton's method (sufficient condition only) is that if

$$\left|\frac{\partial f_1}{\partial m}\right| + \left|\frac{\partial f_1}{\partial h^{+}_{min}}\right| < 1 \qquad (2.22a)$$

and

$$\left|\frac{\partial f_2}{\partial m}\right| + \left|\frac{\partial f_2}{\partial h^{+}_{min}}\right| < 1 \qquad (2.22b)$$

on an interval about the root, the method will converge for any initial values of h^{+}_{min} and m in the interval.

The method of choosing the initial guesses of h^{+}_{min} and m is based on the physical insights from Equation(2.17a). We observed that decreasing h^{+}_{min}, with m held constant, will increase the entire pressure distribution. It is because the term $(1/h^{+3})$ in Equation(2.17) becomes large as h^{+}_{min} decreases. On the other hand, decreasing m, with h^{+}_{min} held

constant, will lower the entire pressure distribution. It is because the term $(h^+-h^+_*)$ in Equation(2.17a) becomes small as m decreases. It was found that pressure was more sensitive to h^+_{min} than to m. After few trials, better initial guesses satisfying the convergence criteria(2.22) are obtained and then used in Newton's method for finding convergent solutions of h^+_{min} and m.

2.7 Results and discussion

Results obtained from the previously described method are presented in Figs(3) and (7). Input data given in Appendix I have been used to obtain these results.

Referring to Figs(3) through (5), it is noted that, at a given speed, the minimum film thicknesses for both rigid and elastic cylinders are decreased as load increases. At very light loads, predictions of minimum film thickness obtained by rigid cylinder theory are in good agreement with the present results. It is because surface deformation under such condition is insignificantly small as compared to the thickness of the film. However, as load increases, deformation becomes increasingly important. Under such cases, the minimum film thickness obtained from the elastohydrodynamic model is found to be much higher than that predicted by rigid cylinder theory. It is simply because cylinder is deformed at increasing loads. It is also observed that ,at higher loads, the minimum film thickness becomes very insensitive to change in load.

It is indicated, from Fig(6), that at a given load, the minimum film thickness is increased as speed increases. This increase in minimum film thickness due to change in speed is found to be quite uniform along any given load.

In order to examine the accuracy of the present results, it is necessary to compare the presently obtained results with the experimental data [15]. For the sake of comparison, $h^+_{min}/(U^+)^{1/2}$ is plotted against $w^+/(U^+)^{1/2}$ as shown in Fig(7). The discrepancy between the present and experimental results at light loads and high speeds is due to the effect of side-leakage. Whereas, the discrepancy at high loads reveals that the assumed film profile is no longer true. However, reasonably good agreement is found in the range of $0.9 \leq w^+/(U^+)^{1/2} \leq 20.0$. Most of the engineering applications in practice fall within this range of loading. Therefore, the described model, based on the concept of Hertzian deformation associated with a tilted-pad configuration shown in Fig(2), is proved to be useful in the analysis of the elastohydrodynamic lubrication of soft materials.

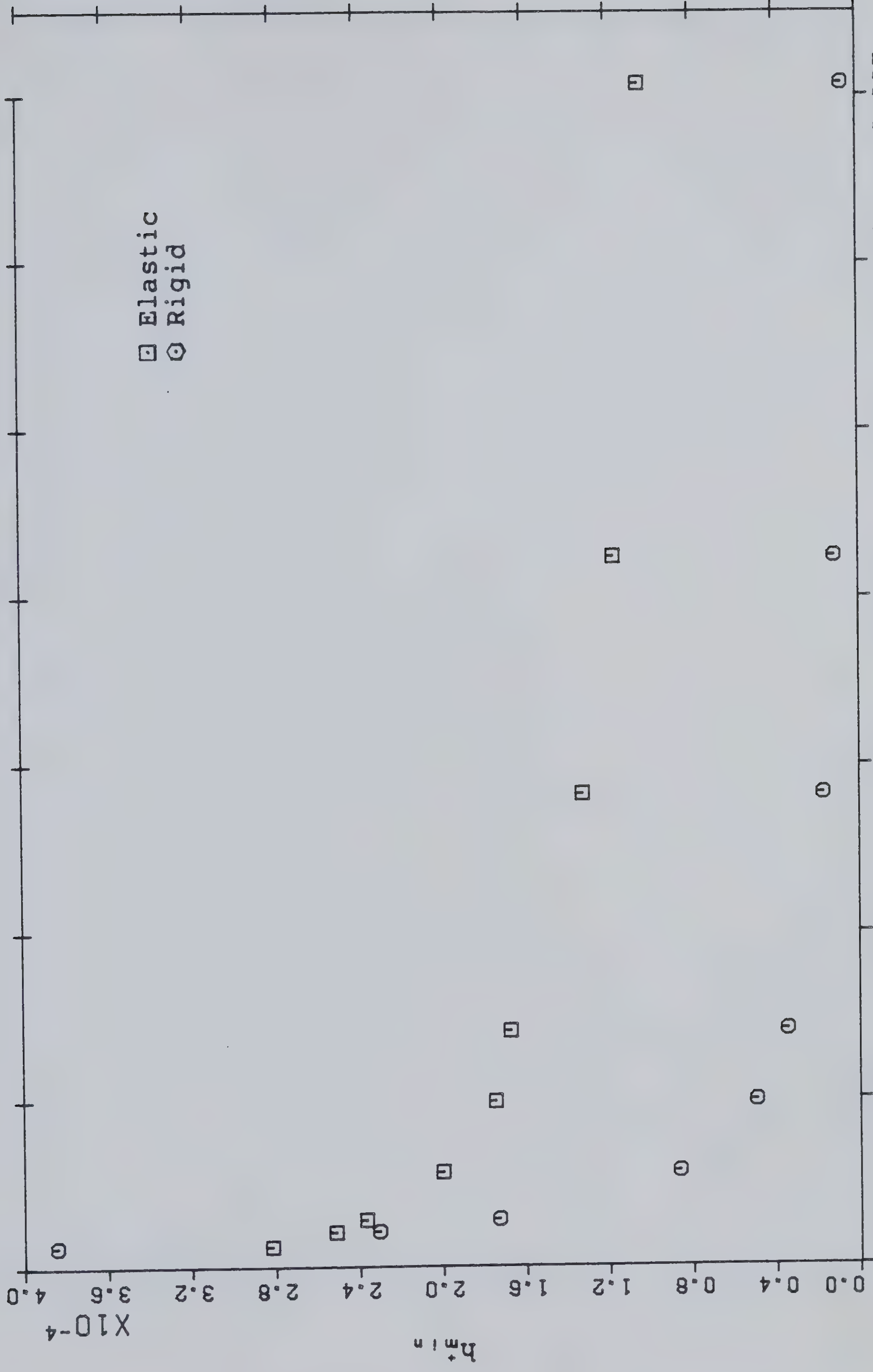

Fig(3) Variation of minimum film thickness with load for $U^+=2\times10^{-8}$

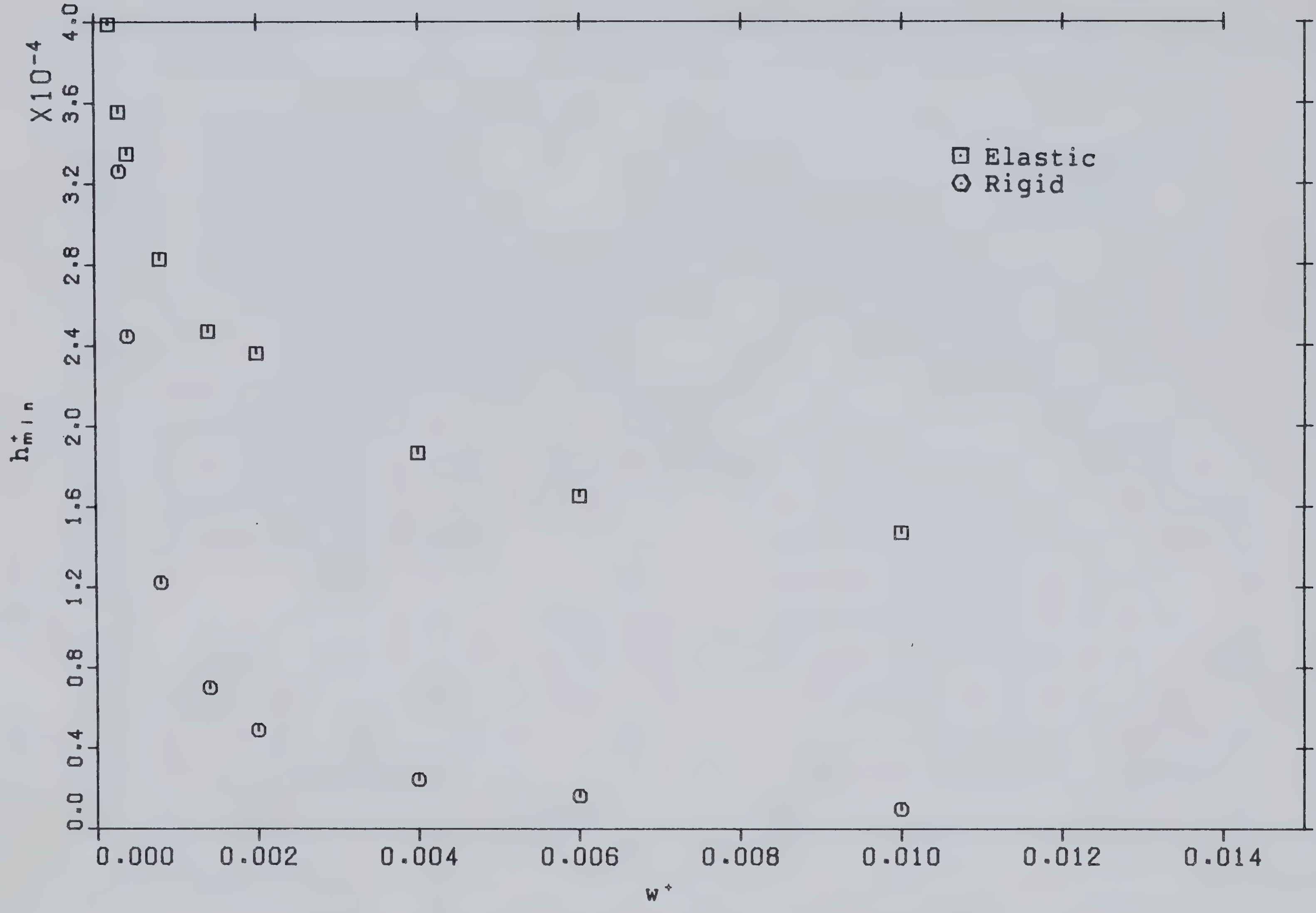

Fig(4) Variation of minimum film thickness with load for $U^+=4x10^{-8}$

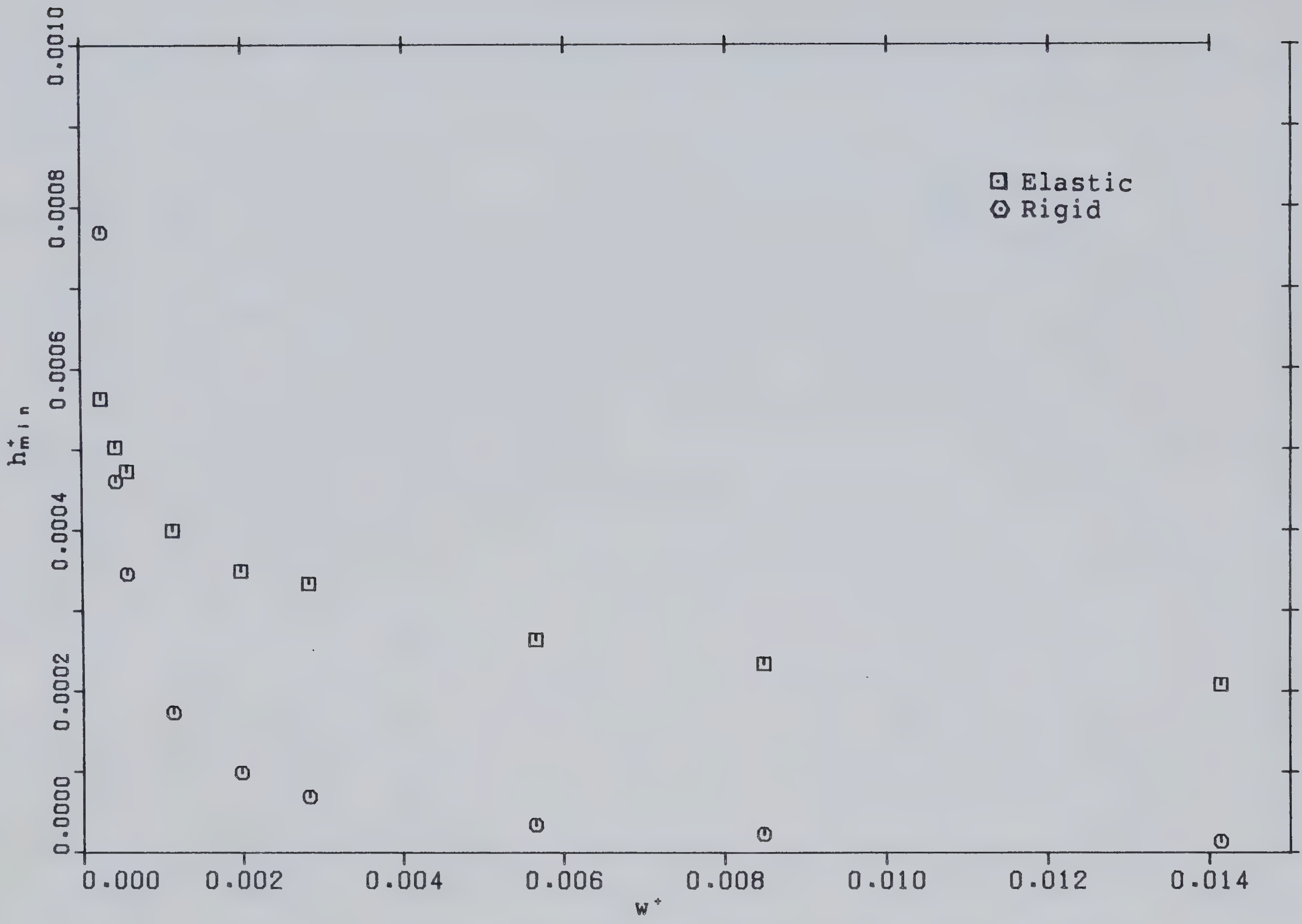

Fig(5) Variation of minimum film thickness with load for $U^{+}=8\times10^{-8}$

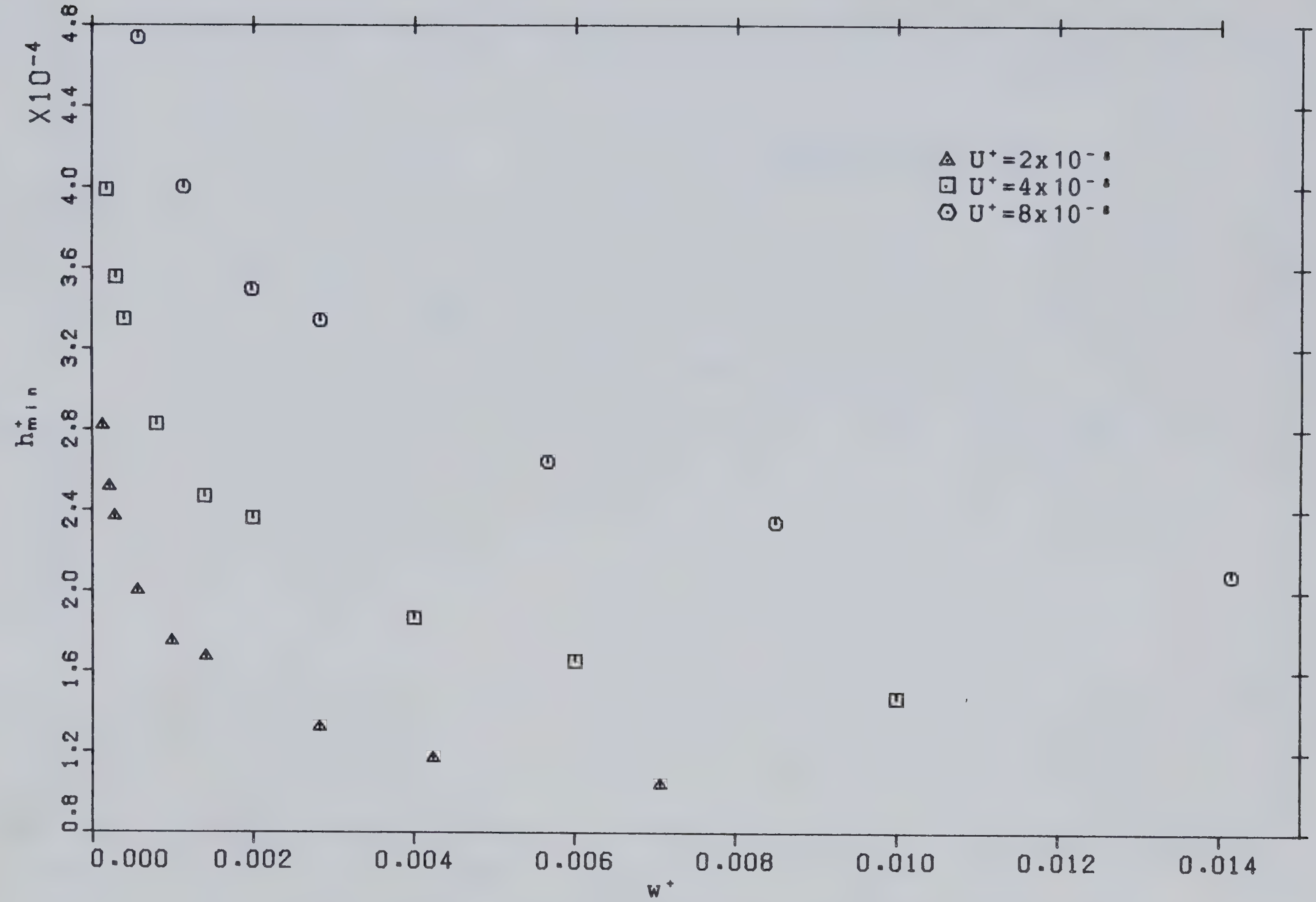

Fig(6) Variation of minimum film thickness with load for various speeds for elastic cylinders

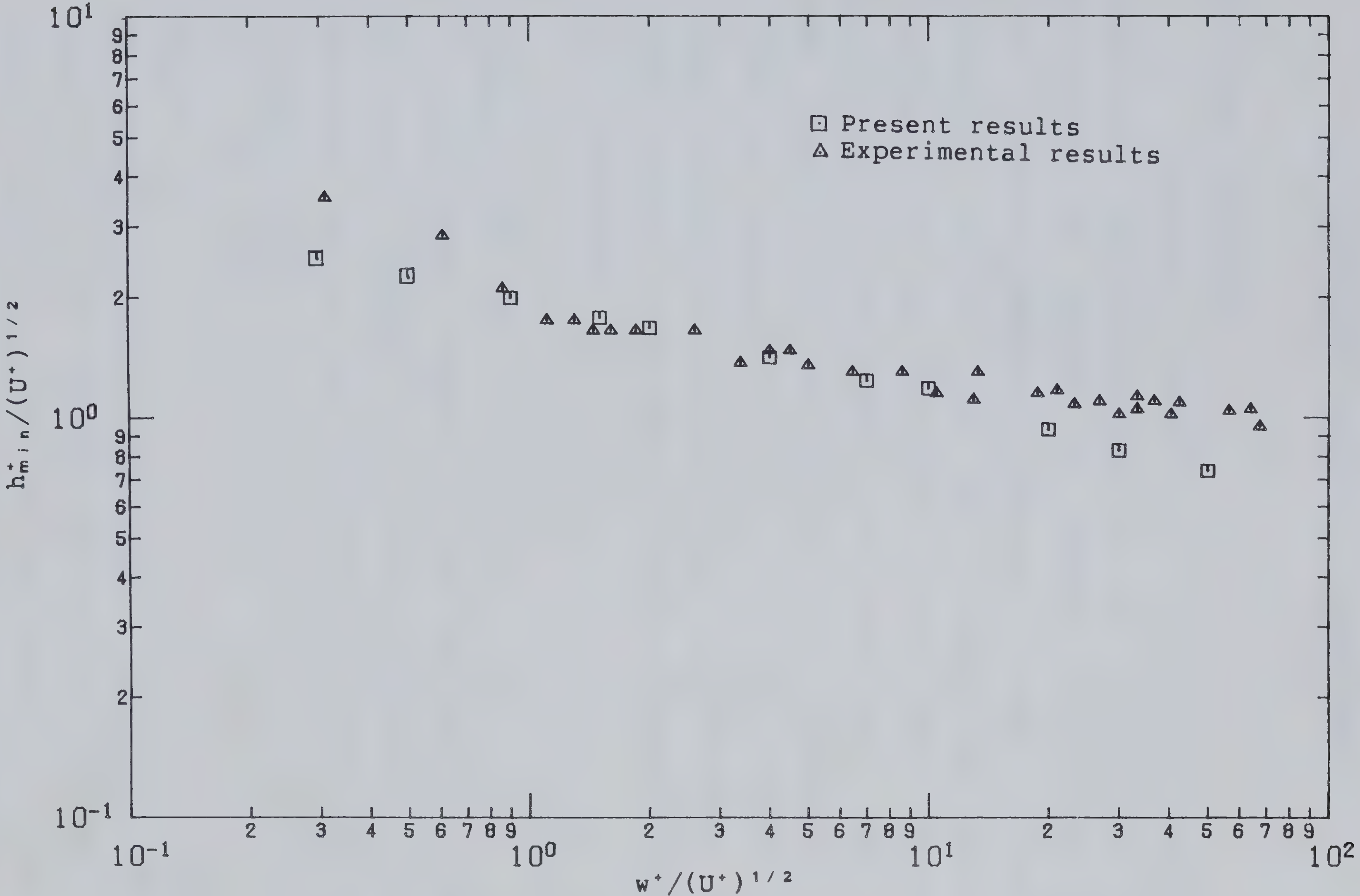

Fig(7) Comparison of present results with experiment

3. THEORETICAL SOLUTION IN LAMINAR REGIME

3.1 General approach

A theoretical solution to the elastohydrodynamic problem must consider the basic equations of elasticity for the solid, and equations of momentum and continuity for fluid. Though the analysis in Chapter 2 yields a useful approximate solution for film thickness and pressure distribution; it does not tell us the actual pressure profile and film thickness in the contact region. Thus, in order to examine the actual details of the problem in a variety of conditions, the basic elasticity, momentum and continuity equations must be solved simultaneously. The initial geometry of the physical problem as shown in Fig(8) will be considered.

3.2 Equations for fluid

As described in Chapter 2, the equations for fluid comprising of momentum and continuity equations may be combined to form one single Equation(2.11) of the form

$$\frac{d}{dx}\left[\frac{1}{\mu}\frac{dp}{dx}\frac{h^3}{12}\right]=-\frac{U}{2}\frac{dh}{dx} \tag{3.1a}$$

where $U=u_1+u_2$ (3.1b)

This equation is based on the assumptions that the flow is laminar, i.e., at low Reynolds number, the viscosity is constant across the film, and the width of the contact region is small compared to the length of the cylinder so

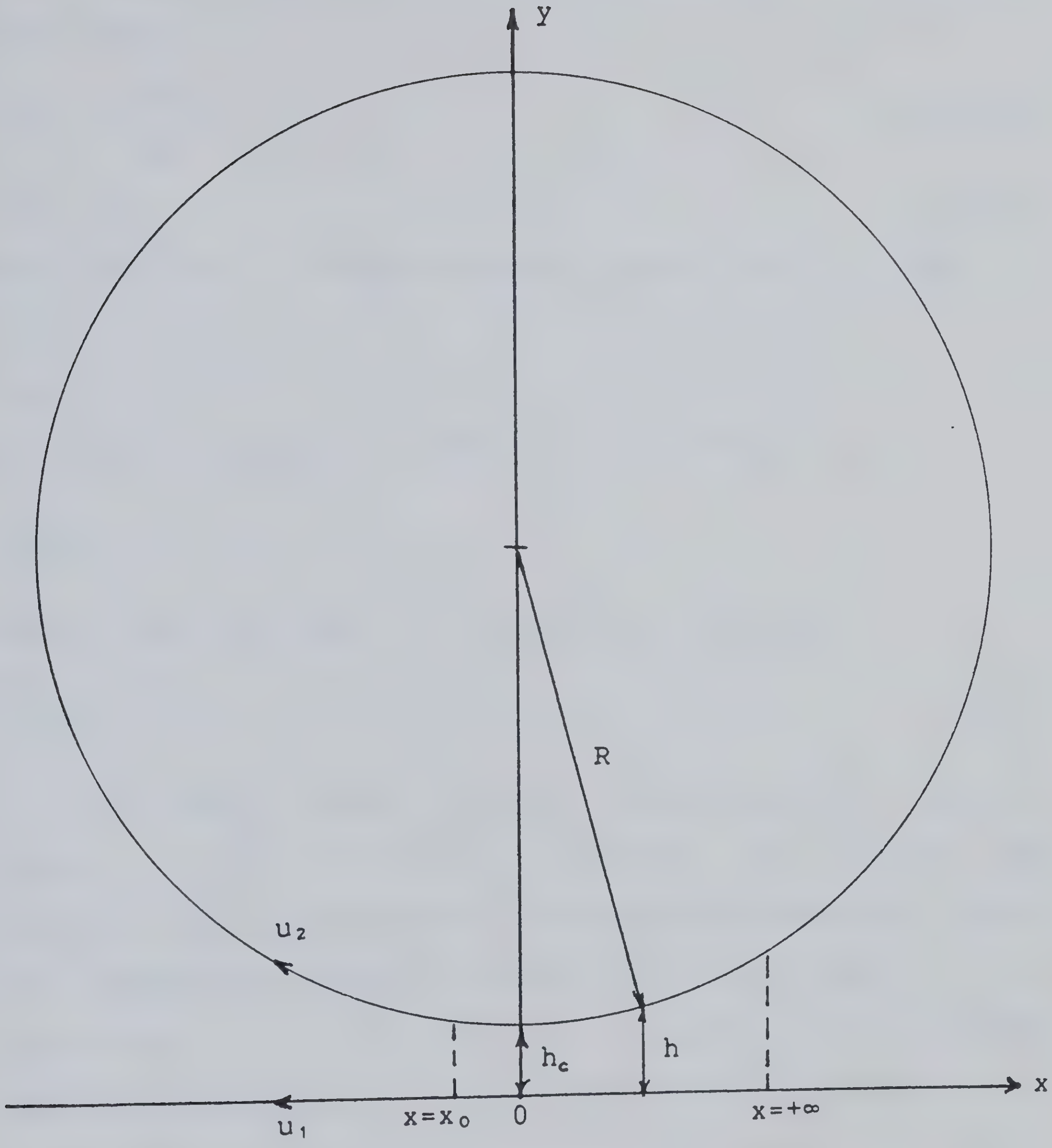

Fig(8) Equivalent cylinder and its coordinate system

that side leakage can be neglected.

The above equation is subject to the following boundary conditions:

$$x=x_0 \;:\; p=\frac{dp}{dx}=0 \tag{3.2a,b}$$

$$x=+\infty \;:\; p=0 \tag{3.2c}$$

Equation(3.1a) is integrated with respect to x, to yield

$$\frac{1}{\mu}\frac{dp}{dx}\frac{h^3}{12}=-\frac{U}{2}h+c_4$$

Now applying boundary condition(3.2b), leads to

$$c_4=\frac{U}{2}h_0$$

Hence integrated form of Equation(3.1a) becomes

$$\frac{dp}{dx}=6U\mu\left(\frac{h_0-h}{h^3}\right) \tag{3.3}$$

At heavily loaded contact, especially in metallic contact, pressure-viscosity effects will arise. The viscosity may be considered to increase exponentially above their atmospheric pressure values, and of the form

$$\mu=\mu_0\exp(\alpha p) \tag{3.4}$$

Introducing Equation(3.4) into Equation(3.3), yields

$$\exp(-\alpha p)\frac{dp}{dx}=6U\mu_0\left(\frac{h_0-h}{h^3}\right) \tag{3.5}$$

Since one of the boundary conditions(3.2) has been used in finding the constant, c_4, Equation(3.5) is therefore only subject to the remaining two boundary conditions:

$$x=x_0 \;:\; p=0 \tag{3.6a}$$

$$x=+\infty : p=0 \tag{3.6b}$$

Now it is convenient to introduce a new variable q [7], known as reduced pressure, such that

$$\frac{dq}{dx}=6U\mu_0\left(\frac{h_0-h}{h^3}\right) \tag{3.7}$$

where

$$\frac{dq}{dx}=\exp(-\alpha p)\frac{dp}{dx} \tag{3.8}$$

Integrating Equation(3.8) with respect to x from the outlet point ,x_0, to some general point ,x, we obtain

$$\int_{q_{x0}}^{q} dq=\int_{p_{x0}}^{p} \exp(-\alpha p)dp \tag{3.9}$$

From the boundary condition(3.6a), p_{x0} is zero. If q_{x0} is set equal to zero, the function q will satisfy the same boundary conditions at x_0 as the pressure, p. Thus from Equation(3.9), we get

$$q=\frac{1}{\alpha}[1-\exp(-\alpha p)] \tag{3.10}$$

It can be readily seen that Equation(3.10) also satisfies the second boundary condition(3.6b). Hence the function q satisfies the same boundary condition as the pressure p, that is

$$x=x_0 : q=0 \tag{3.11a}$$

$$x=+\infty : q=0 \tag{3.11b}$$

Thus this problem can be solved independently. Hence, once Equation(3.7), respresenting the pressure distribution that would occur in an isoviscous lubricant of viscosity μ_0,is

solved then the actual pressure distribution can be found by Equation(3.10). That is

$$p=\frac{1}{\alpha}\ln\left(\frac{1}{1-\alpha q}\right) \tag{3.12}$$

Equation(3.12) is valid only when $\alpha q<1$, i.e. $q<1/\alpha$. If $q>1/\alpha$, the actual pressure goes to infinity. Physically, pressure will never become infinity because high pressure will deform the surfaces into such a shape that the pressure remains finite.

3.3 Elasticity equation

In elastohydrodynamic lubrication situation, it is reasonable to assume that the bounding solids are in a condition of plane strain. It is due to the fact that the width of the pressure region is very small compared with the radius and length of the bounding solids. So the stresses and displacements are uniform along the length, except near the ends. In addition, this fact further allows us to assume that the surface displacements and stresses of the bounding solids can be approximated by those of semi-infinite solids subject to the same normal load. The final film thickness is therefore obtained by adding the vertical displacement to the initial thickness of the film.

First consider a line load on a semi-infinite solid as shown in Fig(9).

Under plane strain condition, i.e. w=constant and $\partial\zeta/\partial z=0$, where ζ is a dummy variable, we obtain

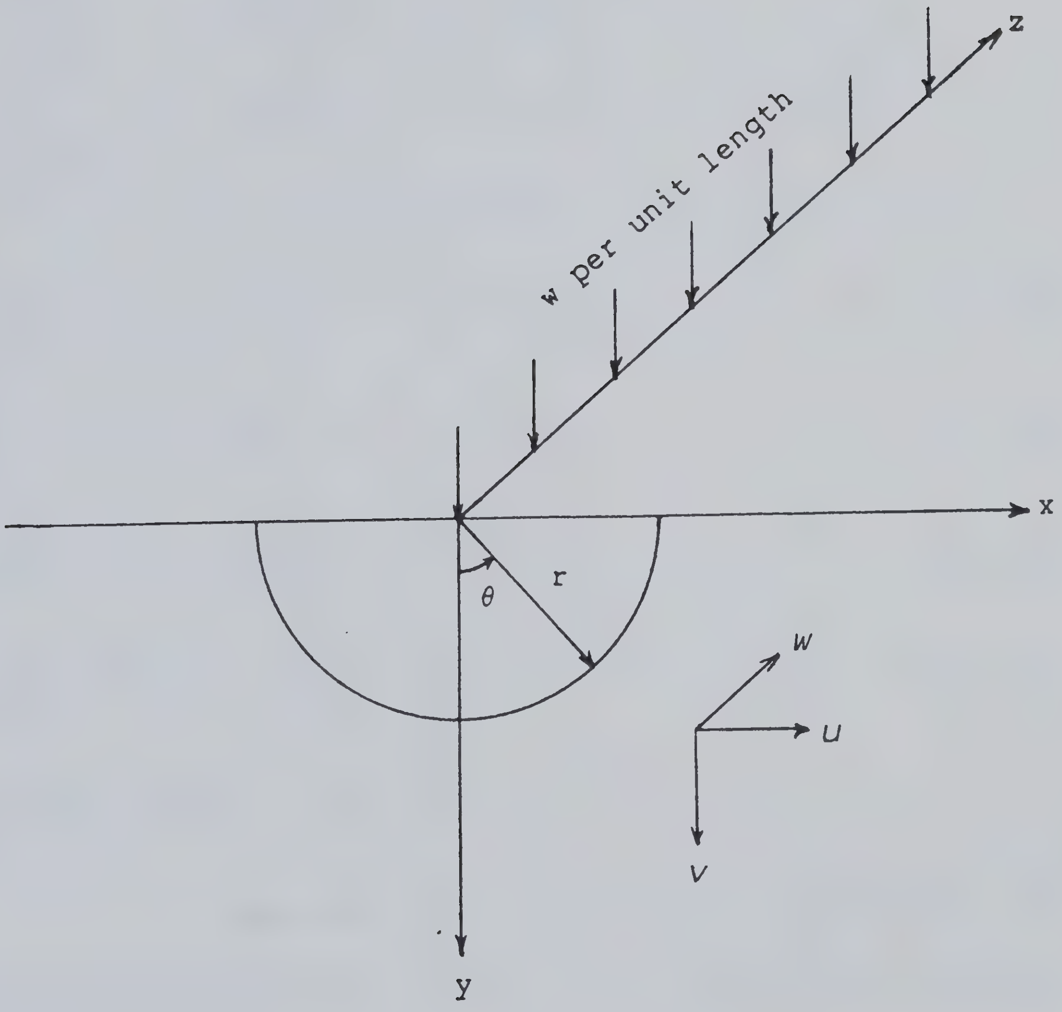

Fig(9) Line load acting on a semi-infinite solid

For direct strain

$$\epsilon_x=\frac{\partial u}{\partial x}\ ,\ \epsilon_y=\frac{\partial v}{\partial y}\ ,\ \epsilon_z=\frac{\partial w}{\partial z}=0$$

For shear strain

$$\gamma_{xy}=\frac{\partial u}{\partial y}+\frac{\partial v}{\partial x}\ ,\ \gamma_{xz}=\frac{\partial u}{\partial z}+\frac{\partial w}{\partial x}=0\ ,\ \gamma_{yz}=\frac{\partial v}{\partial z}+\frac{\partial w}{\partial y}=0$$

Therefore only stresses $\sigma_x,\sigma_y,\sigma_z$ and τ_{xy} are required to be considered.

Hooke's law relates strains to stresses as follows:

$$\epsilon_x=\frac{1}{E}[\sigma_x-\upsilon(\sigma_y+\sigma_z)]=\frac{\partial u}{\partial x} \tag{3.13a}$$

$$\epsilon_y=\frac{1}{E}[\sigma_y-\upsilon(\sigma_x+\sigma_z)]=\frac{\partial v}{\partial y} \tag{3.13b}$$

$$\epsilon_z=\frac{1}{E}[\sigma_z-\upsilon(\sigma_x+\sigma_y)]=\frac{\partial w}{\partial z}=0 \tag{3.13c}$$

$$\gamma_{xy}=\frac{\tau_{xy}}{G}=\frac{2(1+\upsilon)}{E}\tau_{xy}=\frac{\partial u}{\partial y}+\frac{\partial v}{\partial x} \tag{3.13d}$$

From Equation(3.13c) yields

$$\sigma_z=\upsilon(\sigma_x+\sigma_y) \tag{3.14}$$

For a solution to exist, both equilibrium and compatibility equations subject to the appropriate boundary conditions must be satisfied.

Equilibrium equations in two dimensional form are

$$\frac{\partial\sigma_x}{\partial x}+\frac{\partial\tau_{xy}}{\partial y}=0 \tag{3.15a}$$

$$\frac{\partial\sigma_y}{\partial y}+\frac{\partial\tau_{xy}}{\partial x}=0 \qquad (3.15b)$$

Compatibility equation in two dimensional form is

$$\left(\frac{\partial^2}{\partial x^2}+\frac{\partial^2}{\partial y^2}\right)(\sigma_x+\sigma_y)=0 \qquad (3.16)$$

It is convenient to introduce a stress function ϕ (x,y) such that

$$\sigma_x=\frac{\partial^2\phi}{\partial y^2}, \quad \sigma_y=\frac{\partial^2\phi}{\partial x^2}, \quad \tau_{xy}=-\frac{\partial^2\phi}{\partial x\partial y} \qquad (3.17)$$

Equations(3.17) automatically satisfies equilibrium equations(3.15), but the compatibility Equation(3.16) becomes

$$\frac{\partial^4\phi}{\partial x^4}+2\frac{\partial^4\phi}{\partial x^2\partial y^2}+\frac{\partial^4\phi}{\partial y^4}=0 \qquad (3.18)$$

The following Boussinesq stress function satisfies the equilibrium and compatibility equations for the case shown in Fig(9).

$$\phi=-\frac{wr\ \theta\sin\ \theta}{\pi}$$

Then we have the following stress components

$$\sigma_r=\frac{1}{r}\frac{\partial\phi}{\partial r}+\frac{1}{r^2}\frac{\partial^2\phi}{\partial\theta^2}=-\frac{2w}{\pi}\frac{\cos\ \theta}{r}$$

$$\sigma_\theta=\frac{\partial^2\phi}{\partial r^2}=0$$

$$\tau_{r\theta}=-\frac{\partial}{\partial r}\left(\frac{1}{r}\frac{\partial\phi}{\partial\theta}\right)=0$$

These stress equations satisfy the natural boundary

conditions, namely stress free at the surface, i.e. $\sigma_r=0$ at $\theta=90$, except at $r=0$, and $\sigma_r\to0$ as $r\to\infty$.

It is convenient in the present problem to use cartesian coordinates for the stress function and stresses. Stress function becomes

$$\phi=-\frac{w}{\pi}x\tan^{-1}\frac{x}{y}$$

and stress field

$$\sigma_x=\frac{\partial^2\phi}{\partial y^2}=-\frac{2wx^2y}{\pi(x^2+y^2)^2} \tag{3.19a}$$

$$\sigma_y=\frac{\partial^2\phi}{\partial x^2}=-\frac{2wy^3}{\pi(x^2+y^2)^2} \tag{3.19b}$$

$$\tau_{xy}=\frac{-\partial^2\phi}{\partial x\partial y}=-\frac{2wxy^2}{\pi(x^2+y^2)^2} \tag{3.19c}$$

Introducing Equations(3.14) and (3.19) into Equation(3.13a,b) and integrating we get

$$u=-\frac{w}{\pi}[(A+B)\tan^{-1}\frac{x}{y}-(A-B)\frac{xy}{x^2+y^2}]+f(y) \tag{3.20a}$$

$$v=-\frac{w}{\pi}[A\{\ln(x^2+y^2)-\frac{y^2}{x^2+y^2}\}-B\frac{x^2}{x^2+y^2}]+f(x) \tag{3.20b}$$

where $f(y)$ and $f(x)$ are functions of y and x only, respectively; and $A=(1-\upsilon^2)/E$, $B=-\upsilon(1+\upsilon)/E$.

Now by symmetry at any value of y

$$-u(-x)=u(x)$$

Hence $f(y)=0$

To find f(x), Equations(3.13d) and (3.19c)

$$\tau_{xy}=\left(\frac{\partial u}{\partial y}+\frac{\partial v}{\partial x}\right)\frac{E}{2(1+\upsilon)}=-\frac{2wxy^2}{\pi(x^2+y^2)^2} \tag{3.21}$$

Differentiating Equations(3.20) and then introducing them into Equation(3.21), yields

$$\frac{d}{dx}f(x)=0$$

Hence $f(x)=\text{constant}$

Therefore, Equations(3.20) give the displacements anywhere in the body due to a line load at the origin. But we are primarily concerned with the vertical surface displacement, i.e. v at $y=0$, due to a surface pressure p(s) between $x=s_1$ and $x=s_2$ as shown in Fig(10). This displacement can be found by replacing w and x in (3.20b) with (p ds) and (x-s) respectively, and then integrating with respect to s, we get

$$v\Big|_{y=0}=-\frac{(1-\upsilon^2)}{\pi E}\int_{s_1}^{s_2} p(s)\ln(x-s)^2\,ds + \text{constant} \tag{3.22}$$

In the contact between two solids, both surfaces will be deformed by the surface pressure, and if the subscripts 1 and 2 are used to denote the two contacting solids, the sum of the surface displacements become

$$v(x)=-\frac{4}{\pi E'}\int_{s_1}^{s_2} p(s)\ln(x-s)\,ds + \text{constant} \tag{3.23}$$

where

$$\frac{1}{E'}=\frac{1}{2}\left[\frac{(1-\upsilon_1^2)}{E_1}+\frac{(1-\upsilon_2^2)}{E_2}\right]$$

Elasticity equation similar to the one derived above was

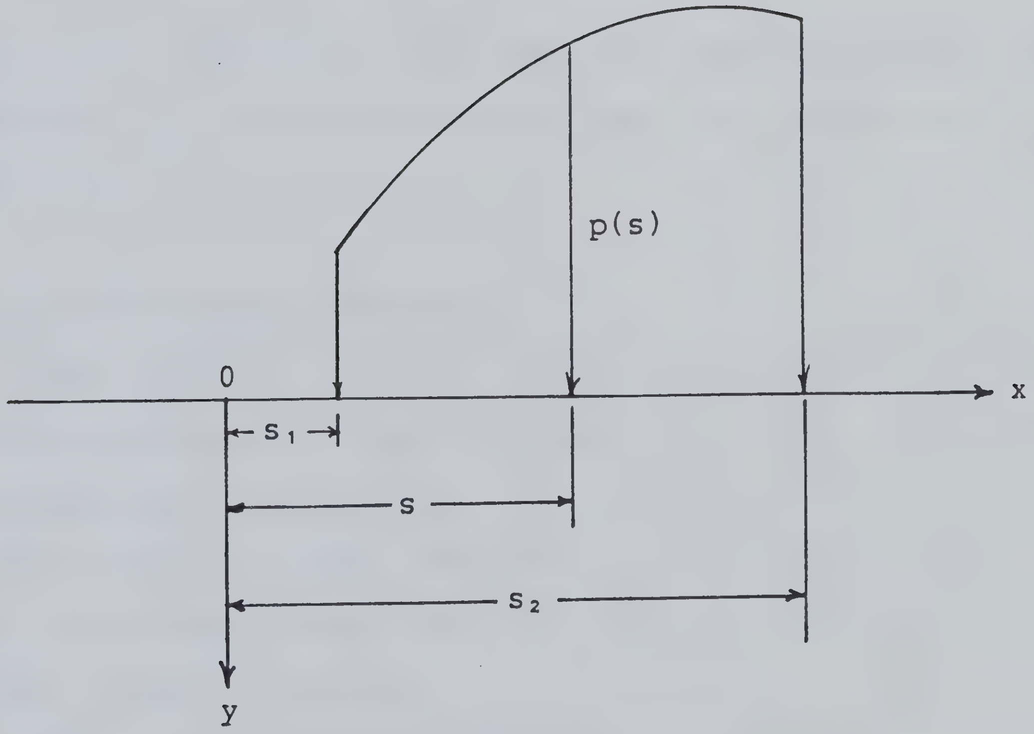

Fig(10)Distributed load between $x=s_1$ and $x=s_2$

also used by Dowson and Whitaker [7] in their analysis of surface displacement.

It is noted that, from Chapter 1, Equation(1.4) represents the film thickness in lubricating rigid contact. Therefore, the resulting film thickness in lubricating elastic contact can be obtained by adding the surface displacement to the undeformed parabolic film thickness, that is

$$h(x)=h_c+\frac{x^2}{2R}+v(x) \tag{3.24}$$

where $v(x)$ is defined by Equation(3.23) and the central film thickness, h_c, can be determined from the lubrication of rigid contact.

3.4 Non-dimensional procedure

Equations(3.7), (3.11), (3.12), and (3.24) can be non-dimensionalized by introducing the following dimensionless variables.

$x^+=x/R$, $q^+=q/E'$, $p^+=p/E'$, $h_0^+=h_0/R$

$h_c^+=h_c/R$, $h^+=h/R$, $g^+=\alpha E'$, $x_0^+=x_0/R$

$v^+=v/R$, $s^+=s/R$, $U^+=U\mu_0/E'R$

Equation(3.7) is non-dimensionalized to

$$\frac{dq^+}{dx^+}=6U^+\left(\frac{h_0^+-h^+}{h^{+3}}\right) \tag{3.25}$$

which is subject to the boundary conditions(3.11) in dimensionless form

$$x^+=x_o^+ \; : \; q^+=0 \tag{3.26a}$$

$$x^+=+\infty \; : \; q^+=0 \tag{3.26b}$$

Equation(3.12) is non-dimensionalized to

$$p^+=\frac{1}{g^+}\ln\left(\frac{1}{1-g^+q^+}\right) \tag{3.27}$$

Equation(3.24) is non-dimensionalized to

$$h^+(x^+)=h_c^+ + \frac{x^{+2}}{2} + v^+(x^+) \tag{3.28a}$$

where

$$v^+(x^+)=-\frac{4}{\pi}\, D(x^+) + C \tag{3.28b}$$

and

$$D(x^+)=\int_{s_1^+}^{s_2^+} [p^+(s^+)\ \ln(x^+-s^+)]\ ds^+ \tag{3.28c}$$

The constant, C, may be determined by specifying the minimum film thickness as will be described in the next section of numerical method. Therefore, from Equations(3.25) to (3.28), the solution depends on three parameters, namely g^+, U^+ and h_{min}^+.

3.5 Numerical Analysis

Numerical techniques of finding the solution for the pressure equation(3.25) subject to the boundary conditions(3.26) with the film thickness equation given by equations(3.28) will be described.

3.5.1 Solution for the pressure equation

It is noted that from the boundary condition(3.26a), the outlet point, x_0^+, is unknown. The way to locate x_0^+ is that by first assuming a value of x_0^+ and applying boundary condition(3.26a) at that point when the pressure equation(3.25) is integrated in the positive x^+-direction. Boundary condition(3.26b) is then checked. If it is not satisfied, a new guess of x_0^+ is tried.

The method of choosing and correcting the assumed value of x_0^+ is based on the fact that moving x_0^+ to the right will decrease the entire pressure distribution, whereas moving x_0^+ to the left will increase the pressure distribution. This will allow us to find upper and lower bounds for x_0^+. Since if the assumed value of x_0^+ is too far right to the actual value, then pressure becomes negative while integrating in the positive x-direction; hence an upper bound. On the contrary, if the assumed value of x_0^+ is too far left to the actual solution, then pressure becomes too high at the inlet; hence an lower bound. Once the bounds for outlet point are found, the solution for x_0^+ can be easily obtained by a simple bisection method.

In actual numerical procedure, it is adopted that $q^+=0$ at $x^+=+\infty$ reaches its asymptotic value when the magnitudes of the pressure and pressure gradient become less than a specified fraction(10^{-3}) of the maximum pressure and maximum pressure gradient, respectively. Equation(1.1a) in Chapter 1 will give a rough guess for the outlet point, x_0^+.

It should be noted that the film thickness is considered to be fixed when x_0^+ is being iterated with the pressure equation(3.25). Once x_0^+ is found, the actual pressure distribution, p^+, can be obtained by Equation(3.27).

3.5.2 Solution for the film thickness equation

Once the pressure distribution is determined for a given initial film thickness, it is time to evaluate a corresponding film thickness variation from Equation(3.28a). This requires the evaluation of the deformation integral $D(x^+)$ in Equation(3.28c). The expression, $D(x^+)$, contains a singularity in the integrand, i.e. $\ln(x^+-s^+)\rightarrow-\infty$ as $x^+\rightarrow s^+$, and so it cannot be evaluated by straight forward numerical integration. This difficulty is removed if the pressure is expressed by a function which enables the integral to be performed analytically. In the present study, $D(x^+)$ is evaluated by dividing the pressure curve into suitable segments. Each segment contains three pressure points and is represented by a second degree polynomial of the form

$$p^+(s^+)=a+bs^++cs^{+2} \qquad (3.29)$$

where a, b, and c are constants for one segment. For the purpose of computation, the origin is taken at the second pressure point of each segment as shown in Fig(11) . Three pressure points of known positions are allocated to each segment and their respective coordinates referring to the new origin can be easily found. With respect to the new

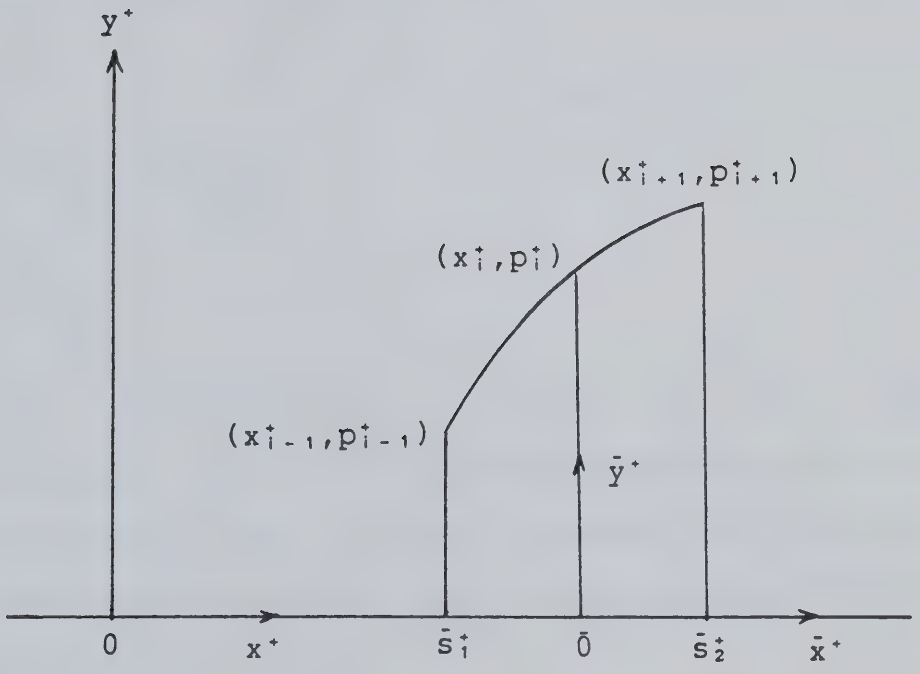

Fig(11)Coordinate system of each pressure segment

origin, the new coordinates for the three pressure points become $(\bar{s}_1^+, p_{i-1}^+)$, $(0, p_i^+)$ and $(\bar{s}_2^+, p_{i+1}^+)$. They are then substituted into Equation(3.29). Consequently, we obtain three similtaneous equations from which constants a, b and c can be determined in each segment. The constants are found to be

$$a=p_i^+$$

$$c=\left(\frac{p_{i+1}^+-a}{\bar{s}_2}-\frac{p_{i-1}^+-a}{\bar{s}_1}\right)\frac{1}{\bar{s}_2-\bar{s}_1}$$

$$b=\frac{p_{i+1}^+-a}{\bar{s}_2}-\bar{s}_2\, c$$

With the pressures, $p^+(s^+)$, in the form of Equation(3.29), we can now integrate Equation(3.28c) without any difficulty. The surface displacements due to each individual pressure segment can be found as described below: For each segment, we have

$$D(\bar{x}^+)=\int_{\bar{s}_1^+}^{\bar{s}_2^+} [(a+b\bar{s}^+ + c\bar{s}^{+2}) \ln(\bar{x}^+-\bar{s}^+)]\, d\bar{s}^+$$

where $\bar{x}^+=x^+-x_i^+$, $\bar{s}_1^+=x_{i-1}^+-x_i^+$ and $\bar{s}_2^+=x_{i+1}^+-x_i^+$

It is noted that the integral

$$\int_{\bar{s}_1^+}^{\bar{s}_2^+} [\bar{s}^{+n} \ln(\bar{x}^+-\bar{s}^+)]\, d\bar{s}^+$$

$$=[1/(n+1)]\{(\bar{s}_2^{+(n+1)}-\bar{x}^{+(n+1)}) \ln|\bar{x}^+-\bar{s}_2^+| - (\bar{s}_1^{+(n+1)}-\bar{x}^{+(n+1)}) \ln|\bar{x}^+-\bar{s}_1^+| - [1/(n+1)](\bar{s}_2^{+(n+1)}-\bar{s}_1^{+(n+1)}) - [1/n]\ \bar{x}^+ (\bar{s}_2^{+n}-\bar{s}_1^{+n}) \ldots\ldots - [1/2]\ \bar{x}^{+(n-1)} (\bar{s}_2^{+2}-\bar{s}_1^{+2}) - \bar{x}^{+n} (\bar{s}_2^+-\bar{s}_1^+)\}$$

Hence, a series of value of $D(\bar{x}^+)$ at a given point x^+ ,where displacement is of interest, can be determined from each

pressure segment. Therefore, the actual displacement due to the entire pressure distribution at the same point x^+ can then be determined by superposing the results of $D(\bar{x}^+)$ obtained from each pressure segment, i.e.

$$D(x^+) = \sum_{m=1}^{k} D(\bar{x}^+) \tag{3.30}$$

where k = total number of pressure segement. Rearranging Equations(3.28), we get

$$(h^+-C)=h_c^+ + \frac{x^{+2}}{2} - \frac{4}{\pi}[D(x^+)]$$

Using Equation(3.30), the function (h^+-C) may be evaluated at every partition point. Then, after the minimum value of this function is found, the proper constant C may be added to the function so as to give the desired minimum film thickness, h^+_{min}.

3.5.3 Film thickness iteration

With the numerical methods described in the above two sections **(3.5.1)** and **(3.5.2)**, we are able to find the pressure distribution from a given film thickness and the film thickness from a given pressure distribution. This procedure allows us to check any given film thickness to see if it is a compatible elastohydrodynamic solution. That is, if a film thickness h_1^+ is given, the corresponding pressure distribution can be obtained from Equations(3.25) and (3.27). The pressure is then used to generate a new film thickness h_2^+ through Equations(3.28). If h_1^+ equal to h_2^+,

then h_1^+ and its associated pressure distribution satisfy the elastohydrodynamic equations. If h_1^+ does not equal to h_2^+, a method of choosing and correcting h_1^+ must be developed so that compatible solution may be obtained. In the present analysis, the resulting film h_2^+ is used as the new guess for h_1^+. This scheme of iterative procedure for film thickness is based on the fact that if the pressure is too high at a given point, there will be too large a deformation and the film thickness will be larger. Thicker films usually result in lower pressures. Hence there is a self-correcting feature for this iterative scheme which should lead to a convergent solution. It was found that the above scheme did not bring convergence in the cases where deformations were large compared to the film thickness. The problem of divergence is removed by introducing a weighting factor, β, which weighs each new film with the previous film. This will prevent too large a change in film thickness in one iteration. Now

$$(h_1^+)_{new} = \beta h_2^+ + (1-\beta)(h_1^+)_{old} \tag{3.31}$$

where the weighting factor $\beta \leq 1$, and $\beta = 1$ represents the original iterative scheme.

As mentioned before in section (3.5.2), the proper constant C may also be added to the new h_1^+ in Equation(3.31) to make the minimum value of h_1^+ agree with the desired minimum film thickness, h_{min}^+, before a new pressure distribution is being iterated.

It was found that either the film thickness, or the maximum pressure or load capacity of the pressure

distribution corresponding to a given film thickness can be used to check for convergence.

The rigid film profile can first be employed to initiate the iterative procedure. However, several iterations are required before a convergent solution can be obtained.

Once the convergent solutions of the film thickness and the corresponding pressure distribution are determined, the load capacity, velocity field and drag force can be obtained from Equations (1.5), (2.10), and (1.7), respectively. The dimensionless form of these equations can be written as follows:

Dimensionless load capacity is of the form

$$w^+=\int_{x_0^+}^{+\infty} p^+dx^+ \tag{3.32}$$

Dimensionless velocity is of the form

$$u^+=\frac{1}{2}\frac{dp^+}{dx^+}(y^{+2}-h^+y^+)+\frac{y^+}{h^+}(u_1^+-u_2^+)-u_1^+ \tag{3.33}$$

Dimensionless drag is of the form

$$F^+=\int_{x_0^+}^{+\infty} \frac{\partial u^+}{\partial y^+}dx^+ \tag{3.34}$$

3.6 Results and discussion

In this section, results obtained from the previously described method will be presented for both low and high elastic modulus materials under four different conditions, namely

(i) rigid cylinder with constant viscosity.

(ii) rigid cylinder with pressure-dependent viscosity.

(iii) elastic cylinder with constant viscosity.

(iv) elastic cylinder with pressure-dependent viscosity.

Input data given in Appendix II has been employed to obtain these results.

As mentioned in the previous section (3.4), results of film thickness and pressure distribution are dependent upon three parameters, namely

(i) minimum film thickness parameter, h^+_{min}.

(ii) speed parameter, U^+.

(iii) pressure-viscosity parameter, g^+.

In the present study, the influence of h^+_{min} and g^+ upon film shape and pressure distribution will be examined.

3.6.1 Results and discussion for soft material

For materials of low elastic modulus, i.e. g^+ becomes small, Figs(12) through (14) show some pressure distributions under four different conditions for three different minimum film thicknesses. To examine the significance of the pressure-viscosity effect, the pressure distributions obtained from constant viscosity are compared with that from pressure-dependent viscosity. It is noted that there is no difference in pressure in both cases. This means that the pressure-viscosity effect may be neglected and only the deformation effect need to be considered in the analysis of lubrication of soft contact. Hence, the

lubricant in such case can be treated as isoviscous fluid. This supports the argument made previously in Chapter 2 that fluid is isoviscous. It is also noted that the pressure distribution obtained from elastohydrodynamic theory is found to be higher than that predicted by rigid hydrodynamic theory. The differences are mostly prominent at small values of h^+_{min}.

It is observed from Fig(15) that as h^+_{min} is lowered, the outlet point starts shifting to the left, resulting in raising the entire pressure distribution. This is caused by deformation of the bounding solid due to the hydrodynamic pressure generated in the fluid film. Maximum pressure is also observed to shift toward the outlet as h^+_{min} decreases. In addition, Fig(15) also shows that small decrease in low values of h^+_{min} can cause a large increase in the entire pressure distribution.

Figs(16) through (18) show the corresponding elastohydrodynamic film thickness for three different values of h^+_{min}. Fig(16) represents the one at lightly loaded conditions, where deformation is relatively small compared to the film thickness. Fig(17) represents the one at intermediate loads, where deformation starts becoming important. It is also noted from Fig(17) that a nearly tilted-pad region is apparent. This supports the argument made previously in Chapter 2 that tilted-pad region does exist for larger loads. Fig(18) represents the one at heavy loads, where deformation is relatively large compared to the

film thickness. The location of h^+_{min} is found to be shifting to the left as h^+_{min} decreases. This accounts for the shift of maximum pressure as mentioned in the previous paragraph.

Velocity profiles at three different locations are shown in Figs(19) through (21). Referring to Fig(19), a linear velocity distribution is noted at the outlet. It is because the pressure gradient at the outlet is zero. In Fig(20), a bulgy parabolic velocity profile is observed at h^+_{min}. This shows the presence of favorable pressure gradient. Fig(21) represents the velocity distribution at the inlet. Back-flow is noted at $y^+>1.2x10^{-2}$. It is due to the presence of adverse pressure gradient.

Figs(22) and (23) respectively show the variations of load and drag for different values of h^+_{min}. As h^+_{min} lowers from $6x10^{-4}$ to $4.5x10^{-4}$, the percentage increases in load and drag are found to be 75% approximately. But as h^+_{min} lowers from $4.5x10^{-4}$ to $3x10^{-4}$, the percentage increases are about 150%. Thus, a trend of rapid rate of increase in load and drag is noted as h^+_{min} gets smaller. The drag at $y^+=0$ is found to be three times the drag at $y^+=h^+$.

3.6.2 Results and discussion for hard material

For materials of high elastic modulus, i.e. g^+ becomes large, pressure distributions under four different conditions for three different minimum film thicknesses are presented in Figs(24), (25) and (26). To study the impact of the pressure-viscosity effect, the comparison between

pressure distributions obtained from pressure-dependent viscosity and constant viscosity is made in the case of rigid cylinder. It is found that there is a significant increase in pressure due to pressure-viscosity effect between $x^+=0.0$ and $x^+=0.02$ for all three values of h^+_{min}. This effect is observed to be increasingly significant with decreasing h^+_{min}. On the other hand, the effect of deformation with constant viscosity is examined. It is noted that pressure distributions obtained from deformation alone are found to be much less than that from pressure-viscosity alone. This shows that the pressure-viscosity effect is more influential than the deformation effect.

Fig(24) suggests that for relatively high values of h^+_{min}, the effect of deformation can be neglected. Only the effect of pressure-viscosity is important. In such cases, the elastohydrodynamic pressure distribution can be accurately obtained by considering the case of rigid cylinder with viscosity varies with pressure. However, Figs(25) and (26) show that as h^+_{min} gets lower, the pressure distribution, obtained by considering pressure-depentent viscosity alone, starts deviating from the true solution. This shows that, even though deformation is small, the effects of pressure-viscosity and elastic deformation are now becoming equally important. Therefore, in order to get an elastohydrodynamic solution, both effects must be considered. The actual maximum pressure is found to be two times higher than that in the case of rigid cylinder with

pressure-dependent viscosity, and is four times higher than that in rigid and elastic cylinders both with constant viscosity. This significantly increase in pressure undoubtedly demonstrates the importance of elastohydrodynamic theory.

Referring to Fig(27), a small decrease in low values of h^+_{min} can give rise to a large increase in the entire pressure distribution. This increase in pressure, however, is not only due to the effect of deformation as described in the previous section for soft materials, but also significantly due to the pressure-viscosity effect. Such an increase in pressure is found to be much drastic in the case of hard material, i.e. g^+ becomes large. The reason is simply due to the influence of pressure-dependent viscosity in hard contact. It is observed that the maximum pressure and the outlet point are slightly shifting to the left with decreasing h^+_{min}. But this shift is not as sharp as that in soft material. The reason is due to the fact that hard material has high elastic modulus, i.e. higher resistance to deformation; therefore, the area subject to deformation is relatively small as compared to that in soft contact. This can be well illustrated in Figs(28) to (30).

Figs(31) through (33) respectively present the velocity profiles at three different locations. Referring to Fig(31), the velocity distribution at the outlet is uniform across the fluid film, since there exists zero pressure gradient. Fig(32) shows that, due to the presence of favorable

pressure gradient, the bullet-shape velocity profile is observed at the place where film thickness is minimum. The maximum velocity occurs at the middle of the minimum thickness of the film and is about 1.6 times higher than the sliding speeds. Furthermore, in order to satisfy the flow continuity, this local maximum velocity must be the global maximum velocity in the entire fluid field. Fig(33) shows the velocity profile at the inlet of the flow. Reverse flow is observed at the central part of the film because of the presence of adverse pressure gradient.

Referring to Figs(34) and (35), variations of load and drag for different minimum film thicknesses are noted. As h^+_{min} lowers from $9.5\text{x}10^{-5}$ to $8\text{x}10^{-5}$, the percentage increases in load and drag are about 39% and 17%, respectively. Whereas, as h^+_{min} lowers from $8\text{x}10^{-5}$ to 6.5^{-5}, the percentage increases are about 128% and 35%, respectively. A tremendous rate of increase in load with small decrease of low values of h^+_{min} is observed. The rate of increase in load is much faster than that found in soft material. The rate of increase in drag is similar to that found in soft contact. It is noted that the drag at $y^+=0$ and $y^+=h^+$ are equal because of the flow symmetry.

In order to study the accuracy of the theoretical results, a comparison is made between the present theoretical results with the earlier experimental and theoretical results obtained by others. For the sake of comparison, $h^+_{min}/(U^+)^{1/2}$ is plotted against $w^+/(U^+)^{1/2}$ as

shown in Figs(36) and (37). Reasonably good agreement is found.

4. CONCLUSION

A study was made on an isothermal elastohydrodynamic lubrication of materials of both low and high elastic moduli. The described physical model, based on the concept of Hertzian deformation associated with a tilted-pad surface, for materials of low elastic modulus was proved to be useful in predicting the minimum film thickness, $h^+_{min}/(U^+)^{1/2}$, over a wide range of loads, $w^+/(U^+)^{1/2} = 0.9$ to 20. In the range of conditions where elastic deformation was important, it was found that for a given load and speed, the minimum film thickness was much greater than the rigid cylinder theory would indicate. The increase in minimum film thickness due to change in speed was found to be quite uniform along any given load.

Results obtained from the theoretical analysis indicated that for lubrication of soft materials with $g^+=0.933$, the effect of pressure-dependent viscosity could be neglected. Only the effect of elastic deformation should be considered in such cases. However, for lubrication of hard materials with $g^+=3000$, both effects of pressure-viscosity and elastic deformation were found to be equally important in the generation of the resulting pressure distribution. Over the range where deformation became important, it was noted that for a given minimum film thickness and speed, load capacity was much higher than that obtained by rigid cylinder theory. Drag and load were found to be increased with decreasing minimum film thickness.

Small decrease in low values of the minimum film thickness would cause a large increase in load. In other words, when deformation is significant, minimum film thickness was slightly dependent on load.

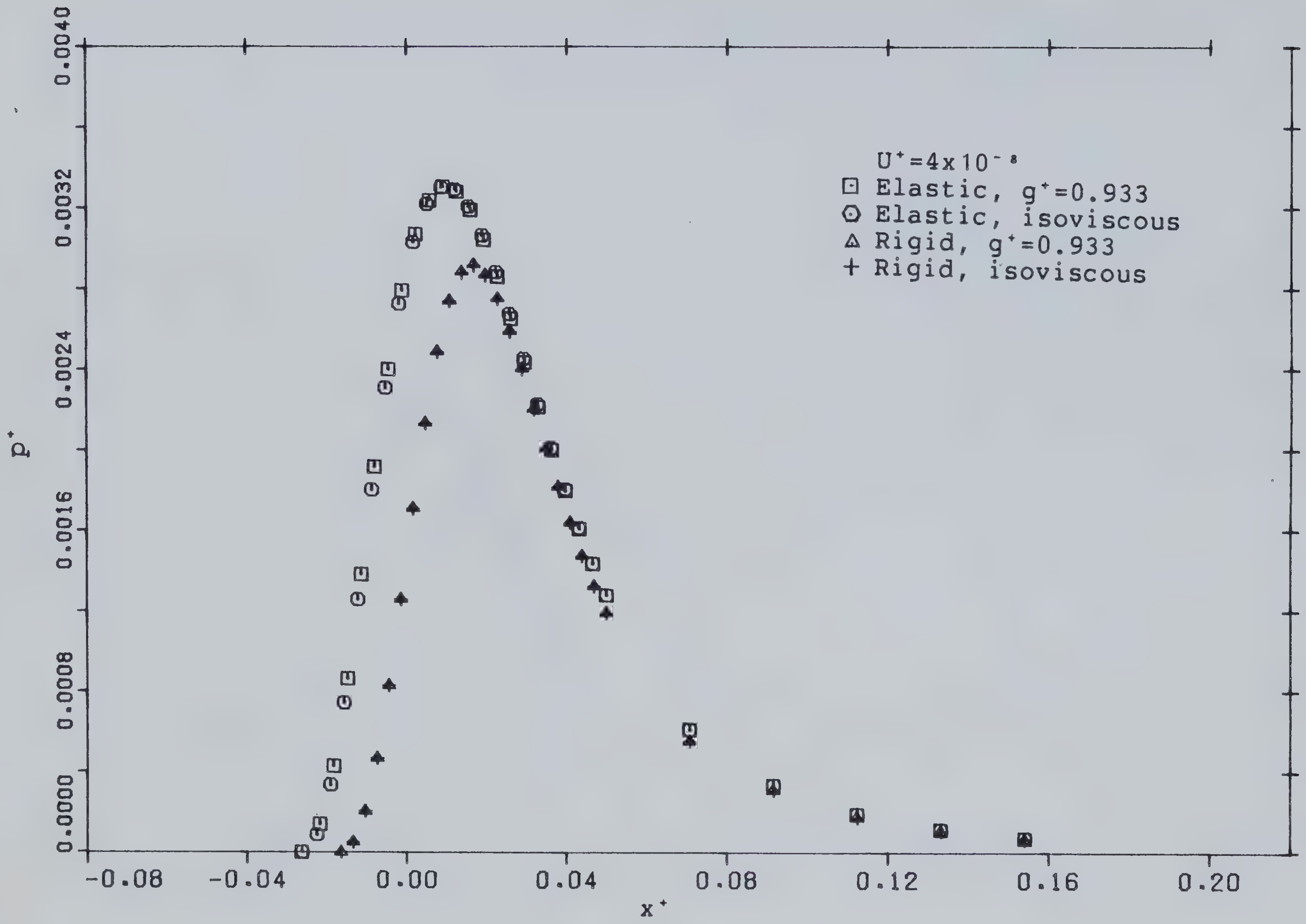

Fig(12) Pressure distributions for $h^{+}_{min}=0.6\times10^{-3}$

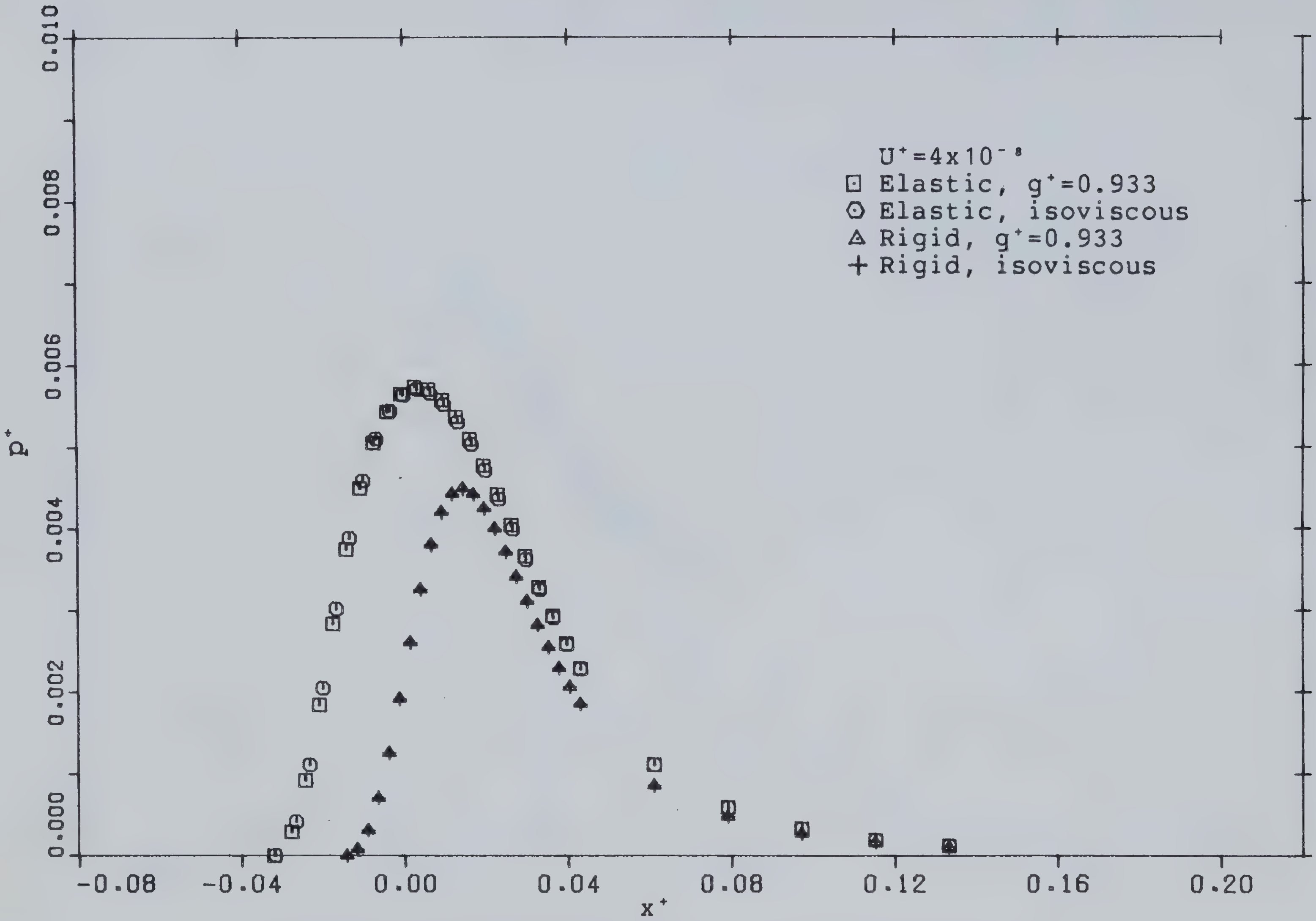

Fig(13) Pressure distributions for $h^+_{min}=0.45\times10^{-3}$

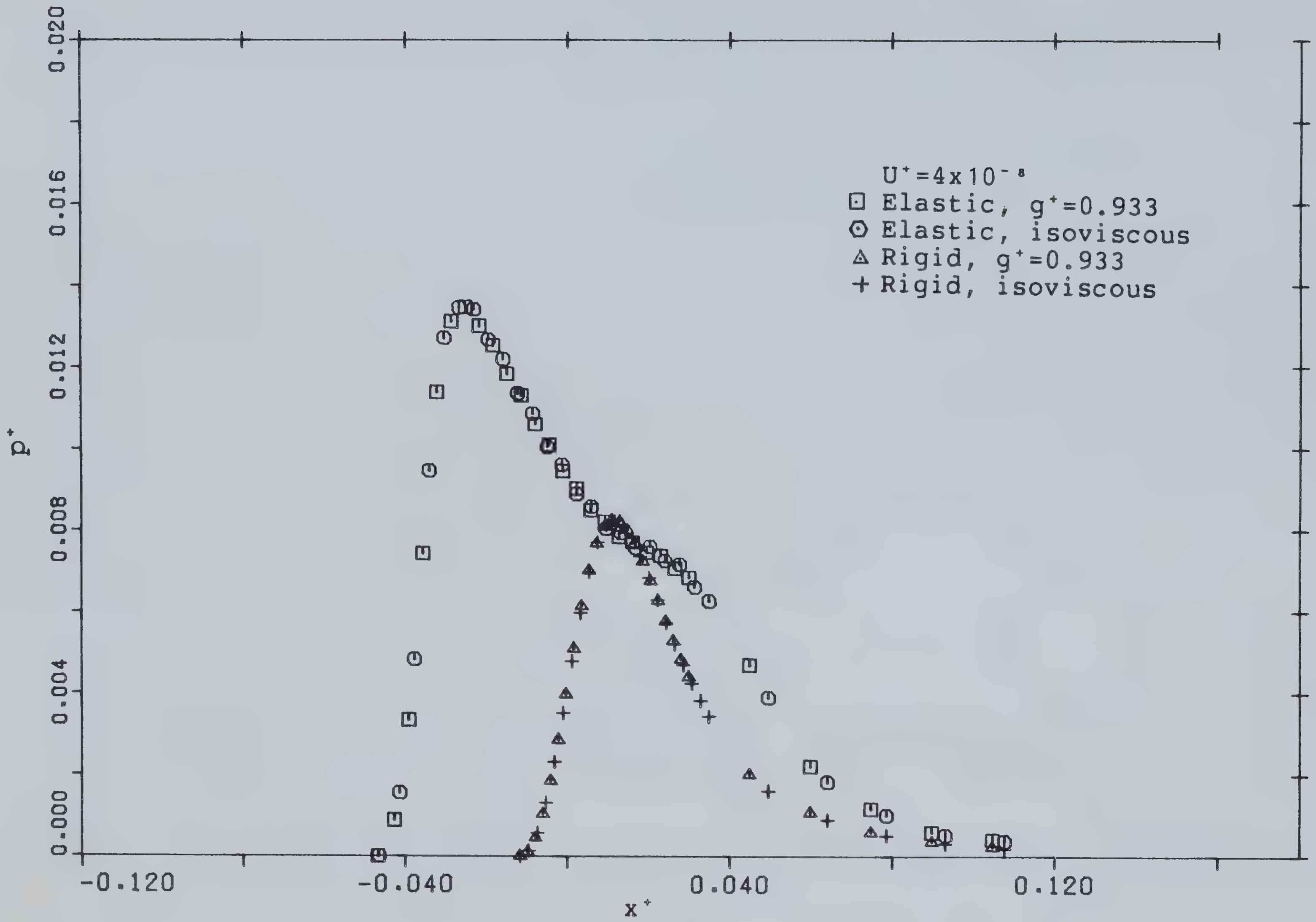

Fig(14) Pressure distributions for $h^{+}_{min}=0.3\times10^{-3}$

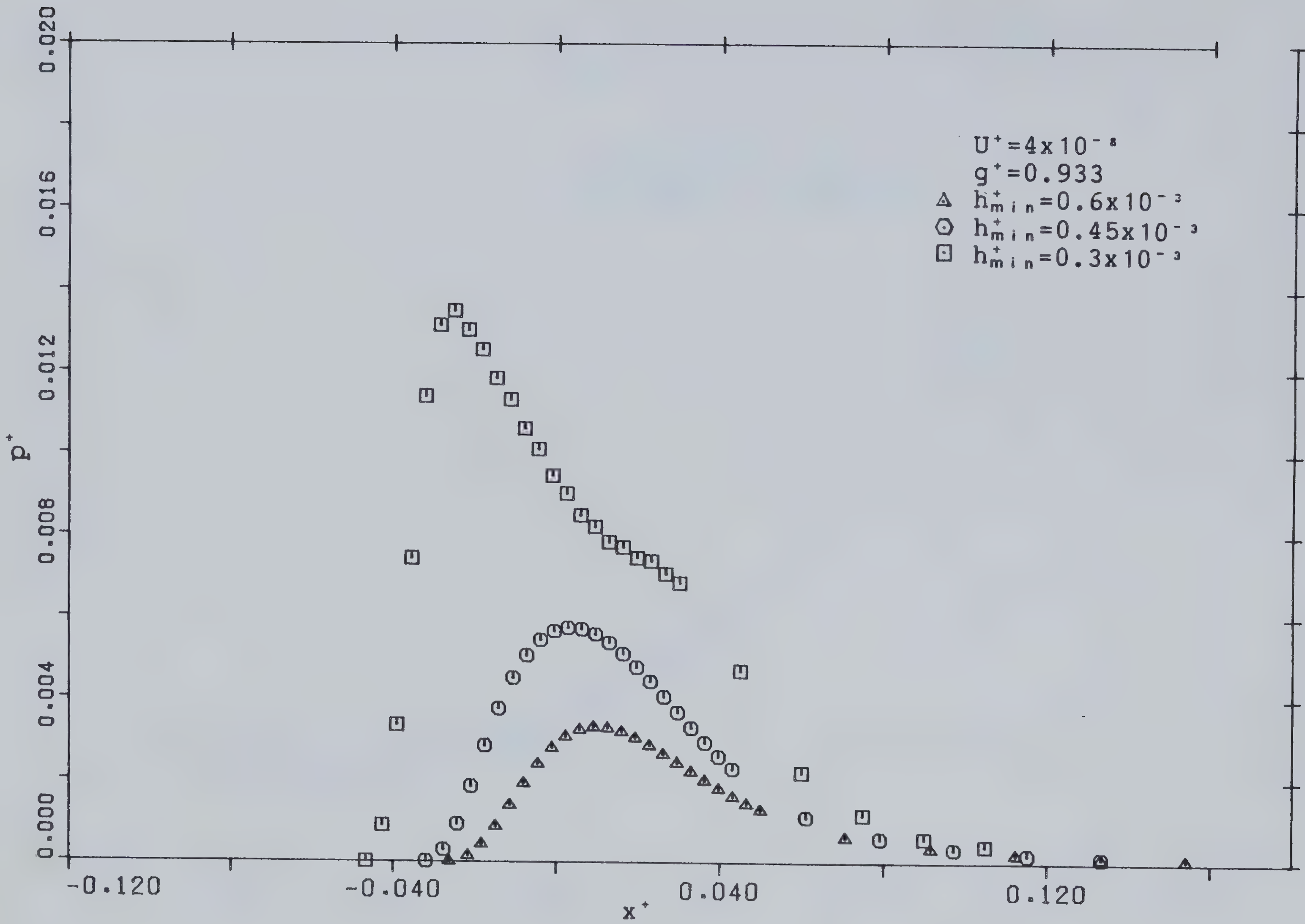

Fig(15) Pressure distributions for various h^{+}_{min}'s for elastic cylinder

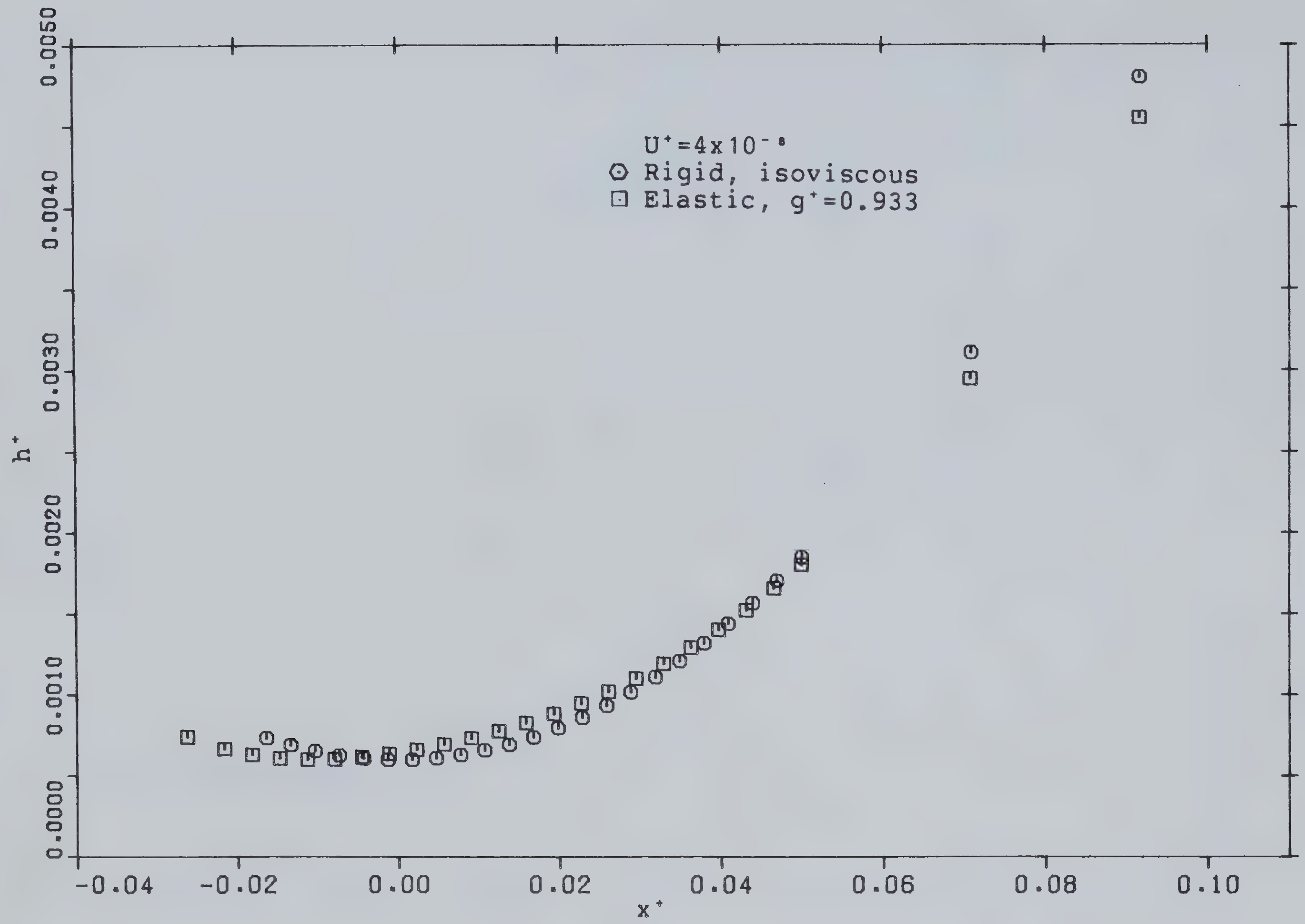

Fig(16) Film thickness variation for $h^+_{min}=0.6\times10^{-3}$

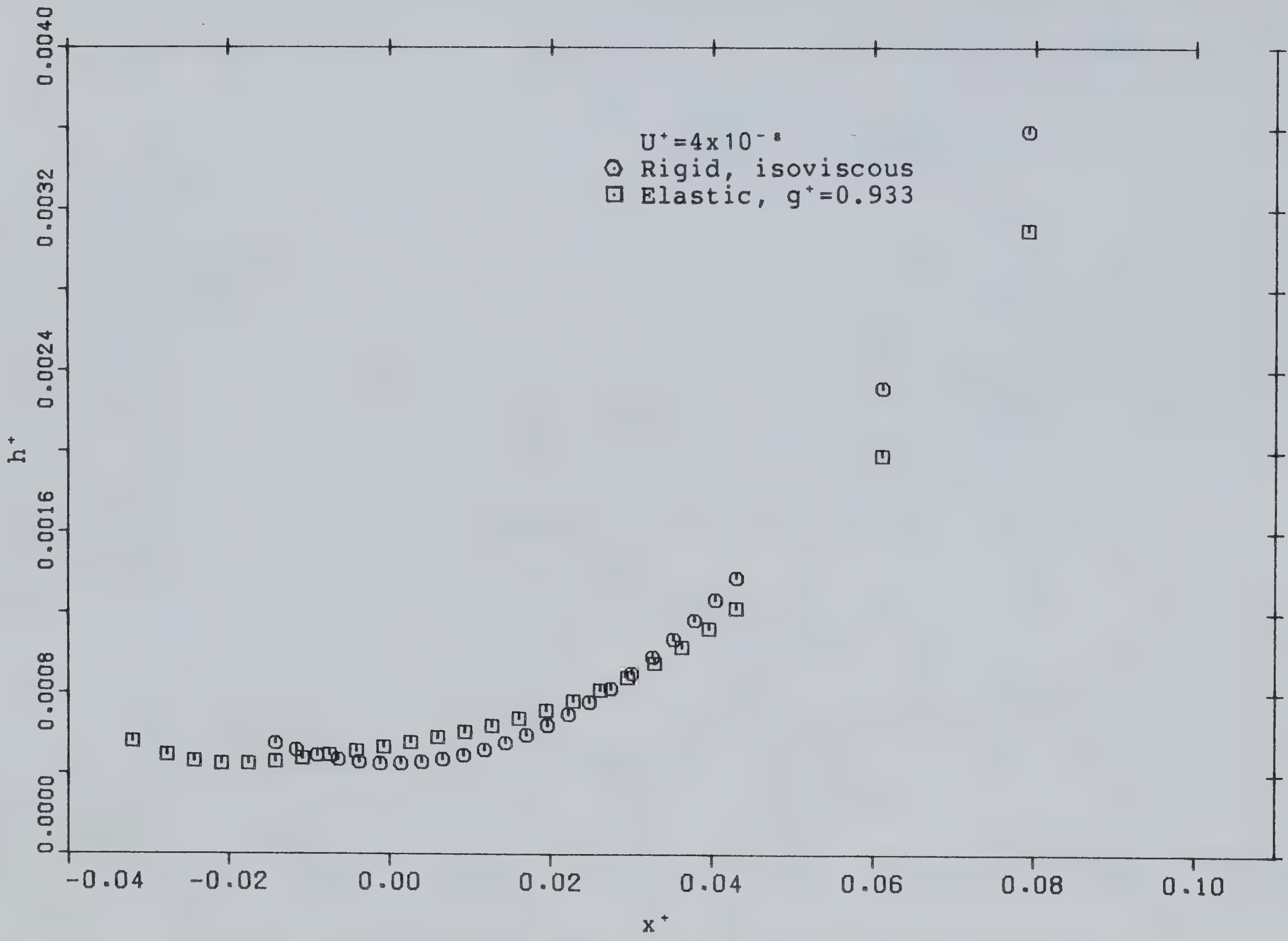

Fig(17) Film thickness variation for $h^+_{min}=0.45\times10^{-3}$

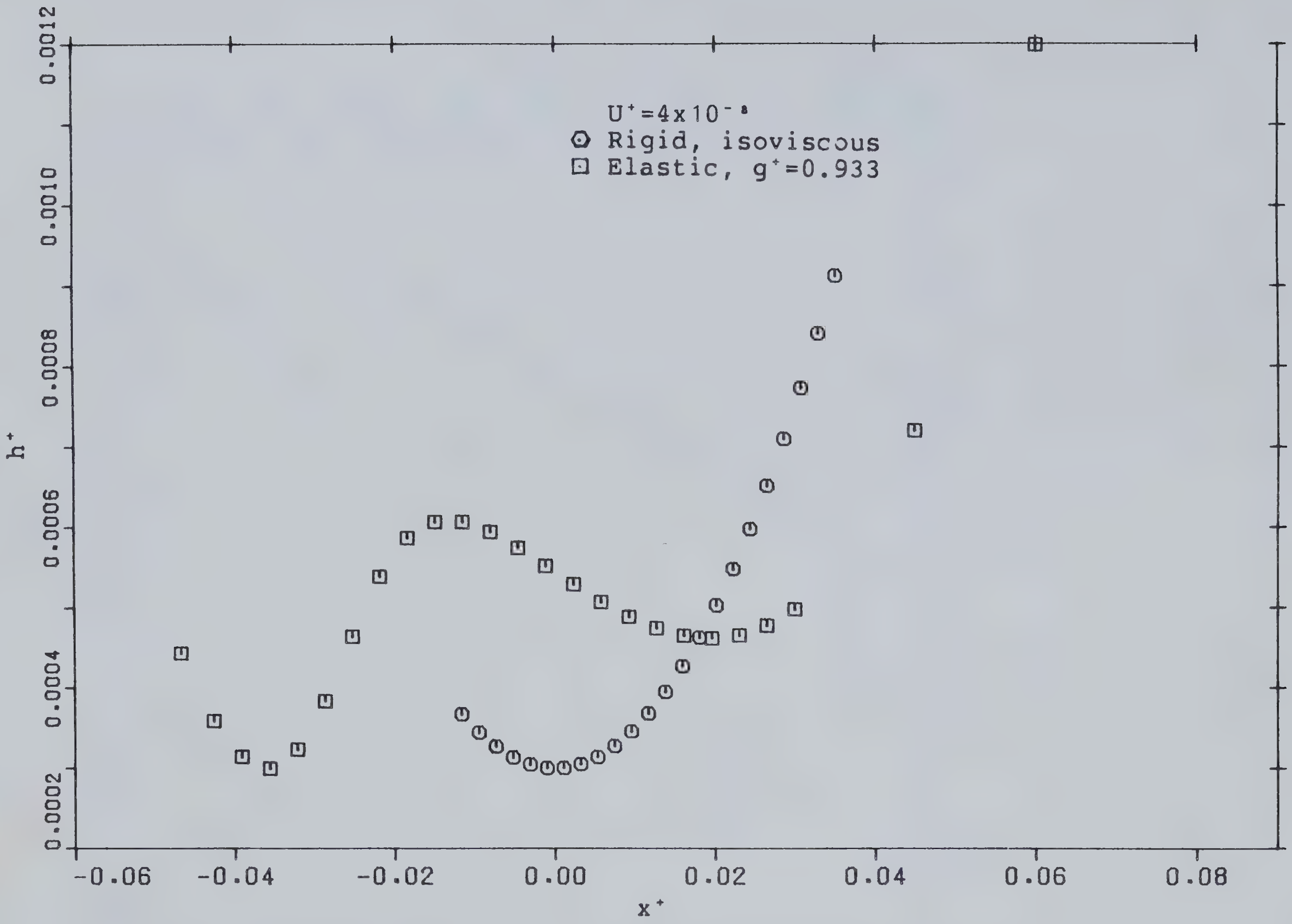

Fig(18) Film thickness variation for $h^+_{min}=0.3\times10^{-3}$

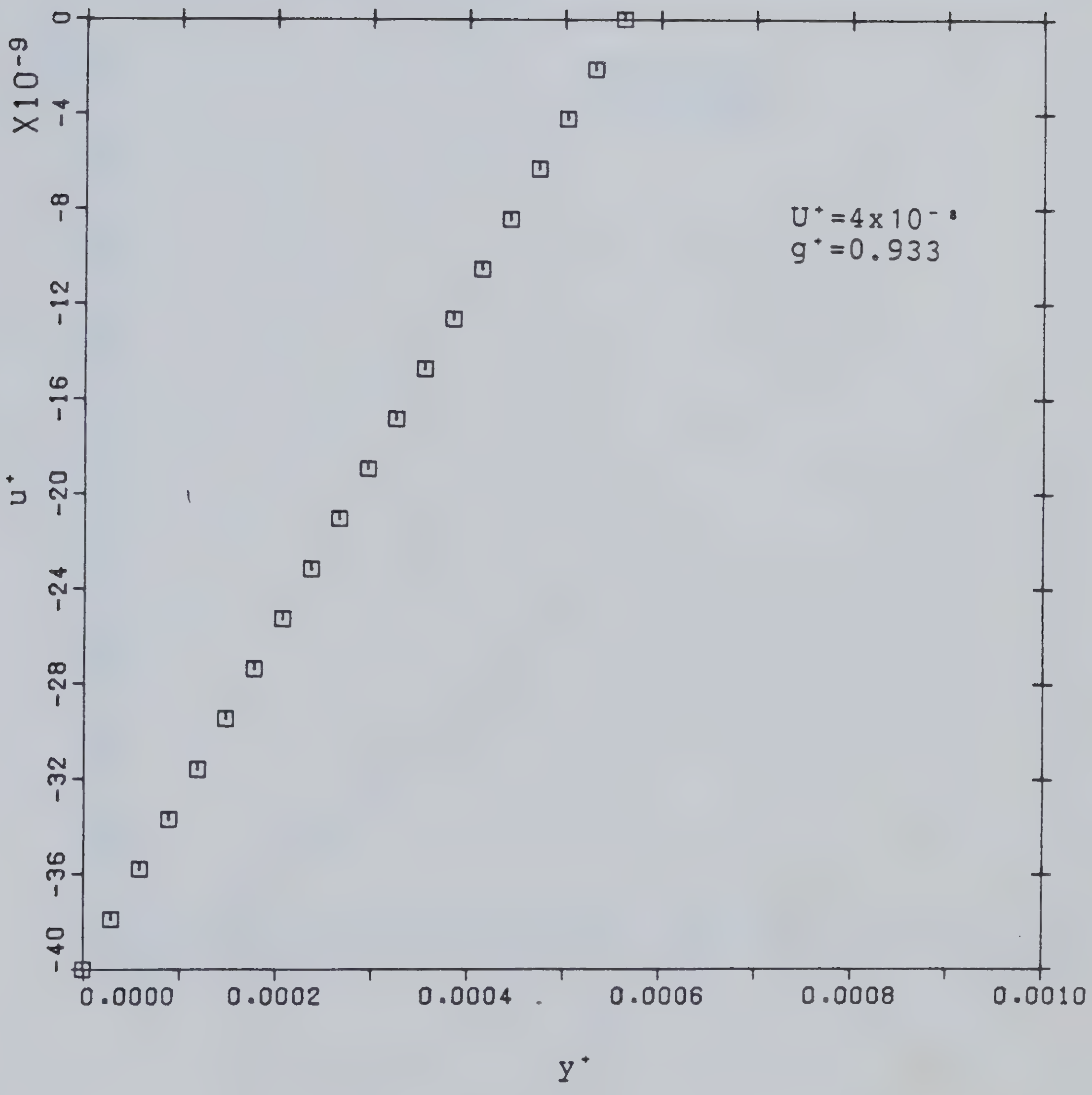

Fig(19) Velocity distribution at outlet for $h^+_{min}=0.45\times10^{-3}$ for elastic cylinder

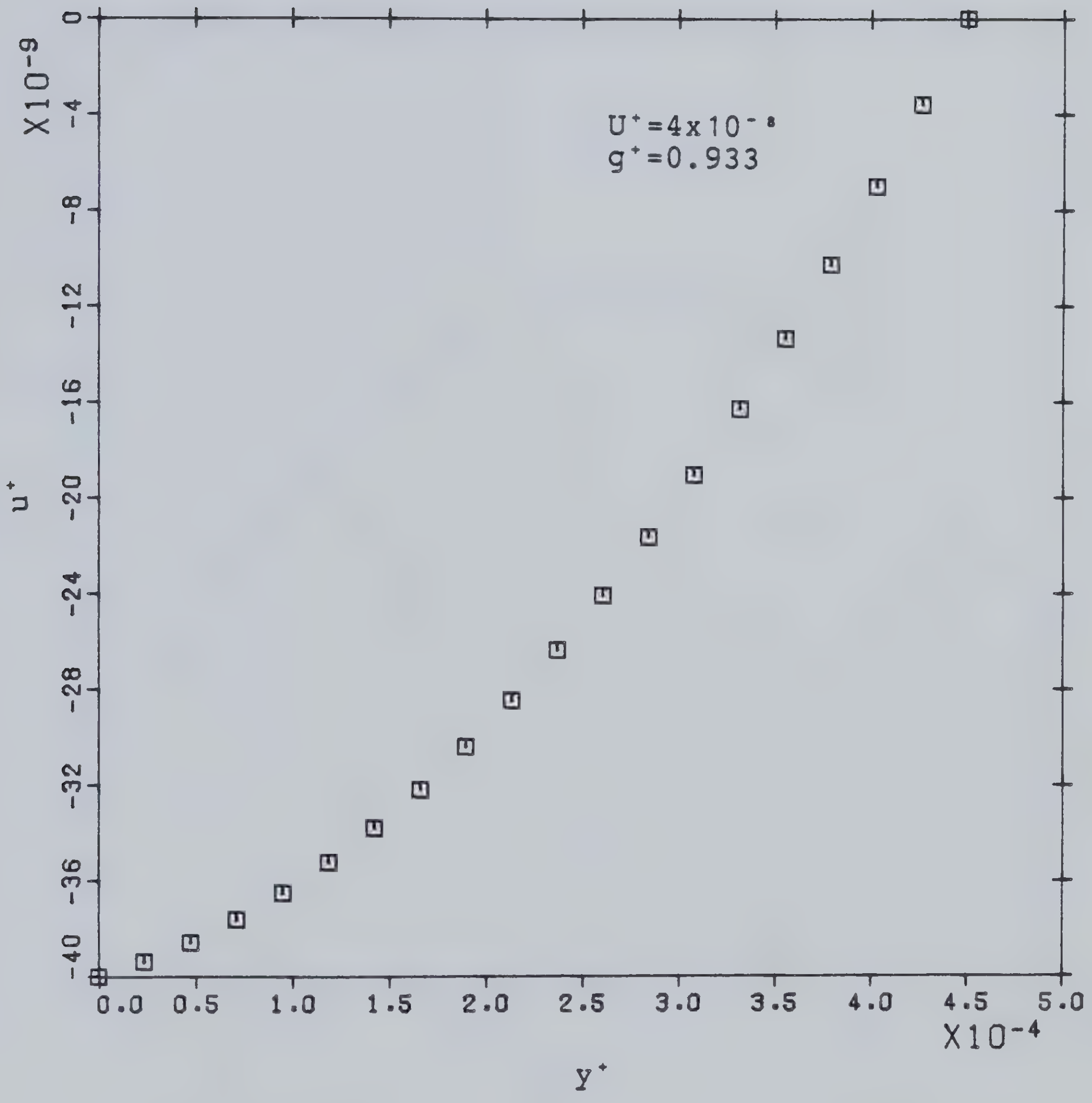

Fig(20) Velocity distribution at which h is minimum for $h^{+}_{min}=0.45\times10^{-3}$ for elastic cylinder

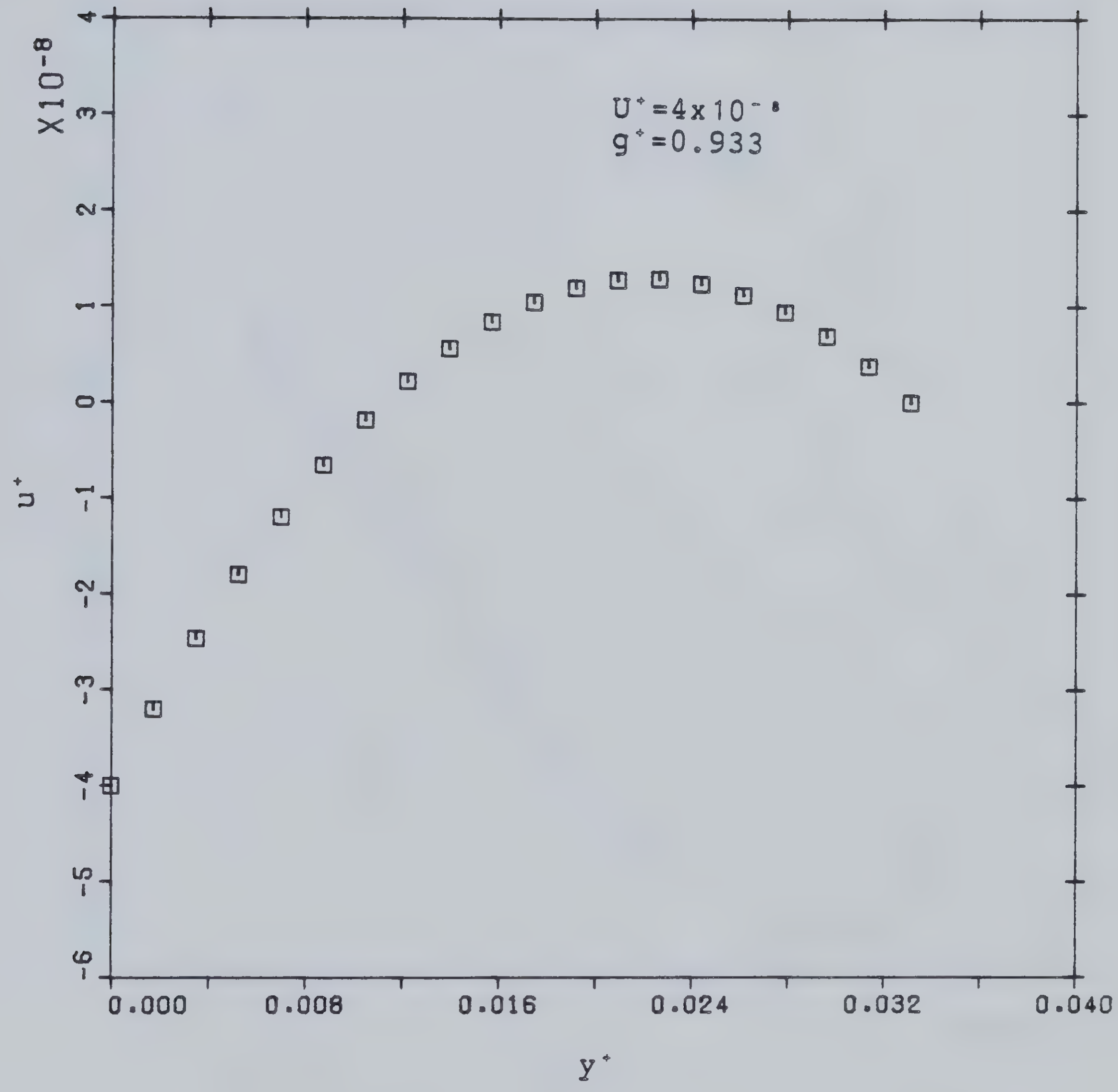

Fig(21) Velocity distribution at inlet for $h^{+}_{min}=0.45\times10^{-3}$ for elastic cylinder

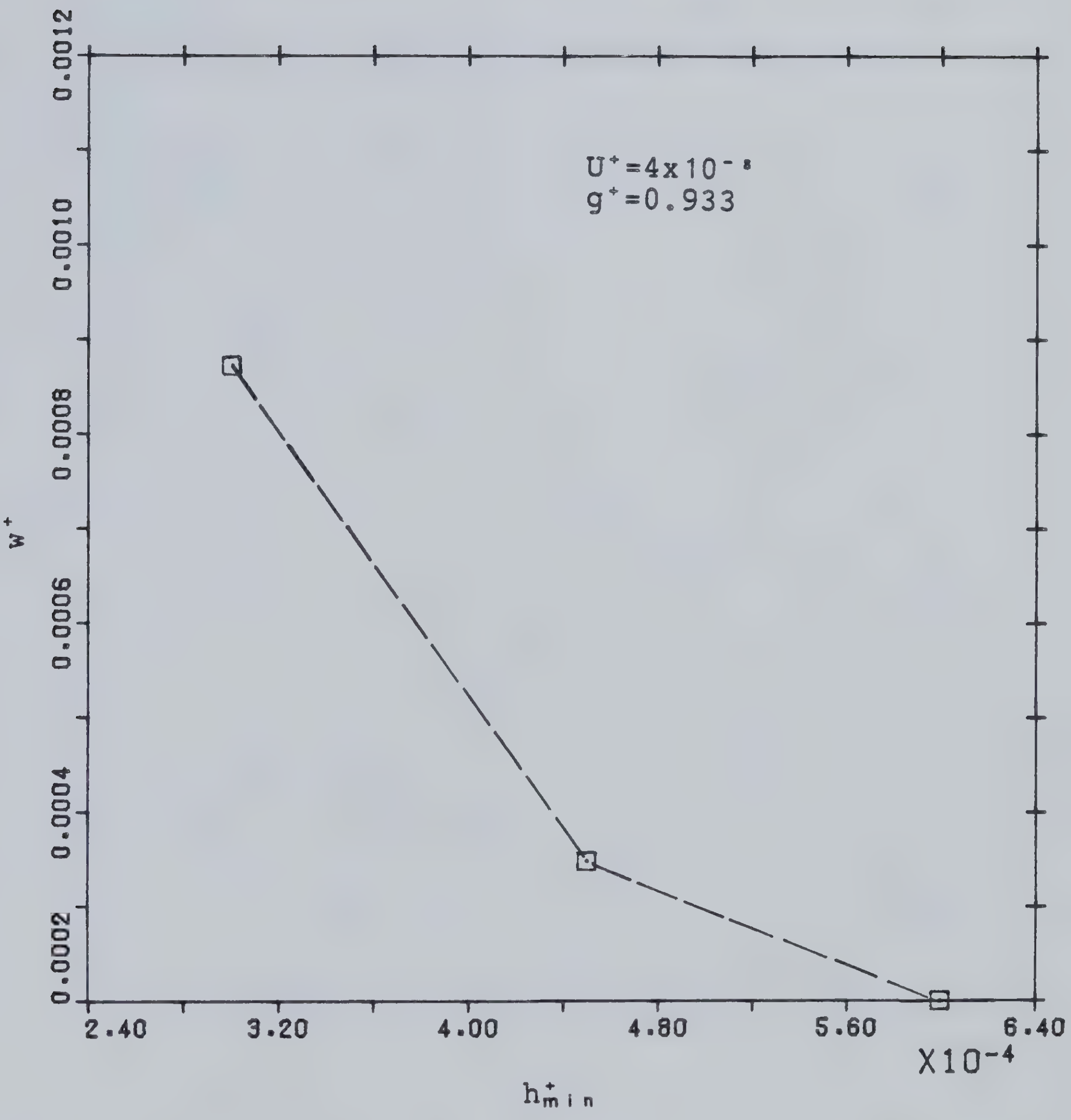

Fig(22) Variation of load with minimum film thickness for elastic cylinder

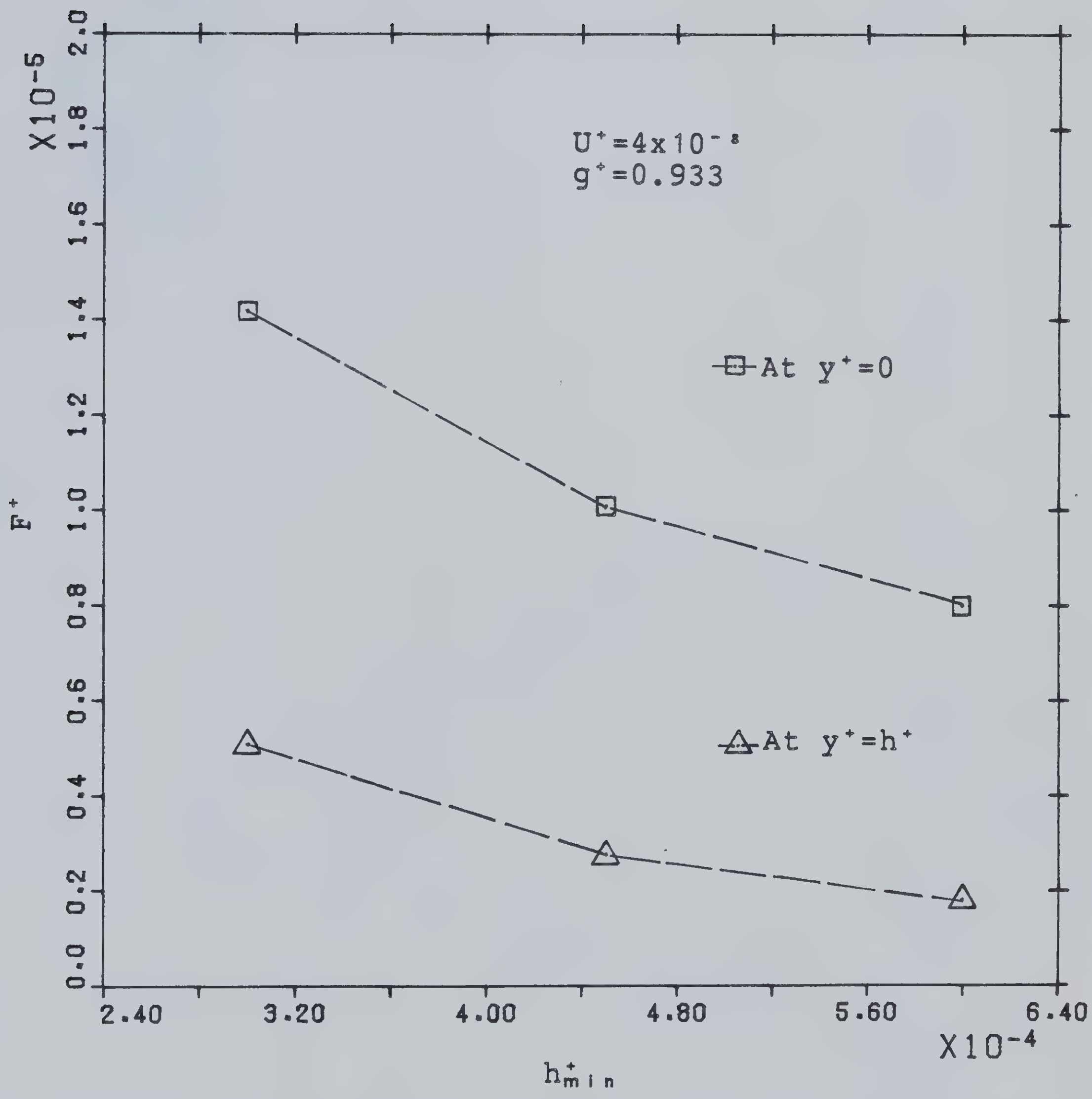

Fig(23) Variation of drag with minimum film thickness for elastic cylinder

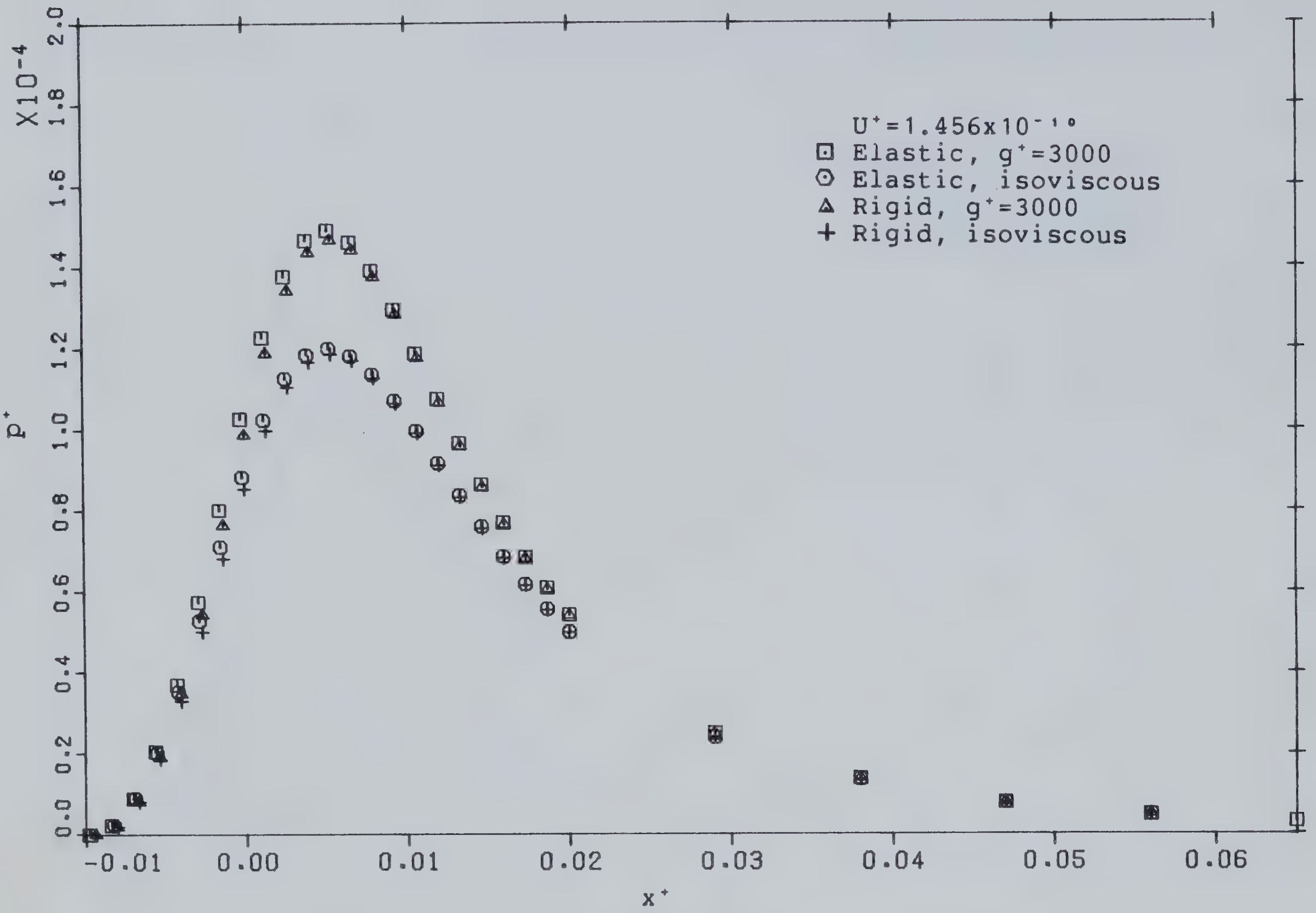

Fig(24) Pressure distributions for $h^{+}_{min}=1.2\text{x}10^{-4}$

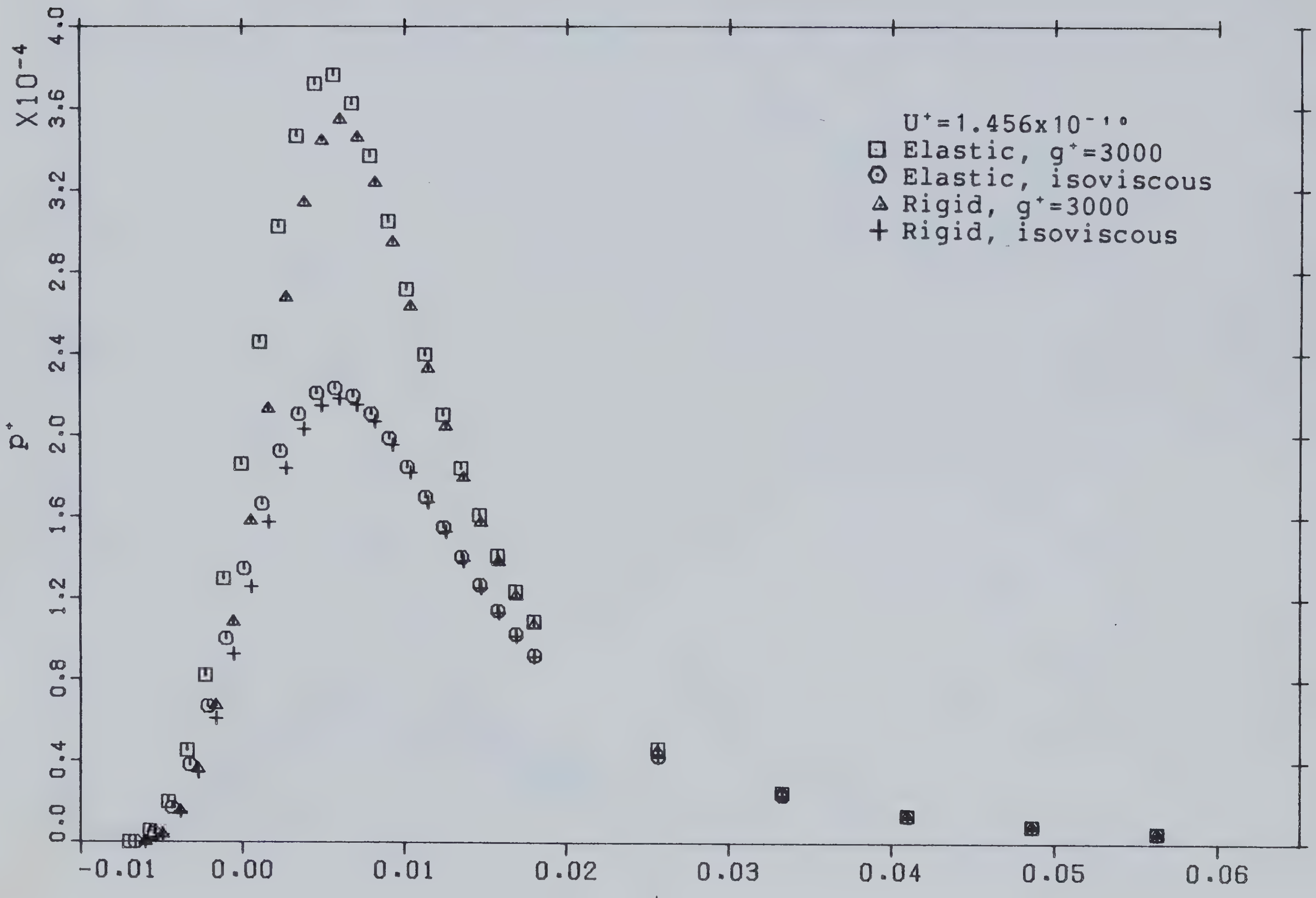

Fig(25) Pressure distributions for $h^+_{min}=0.8\times10^{-4}$

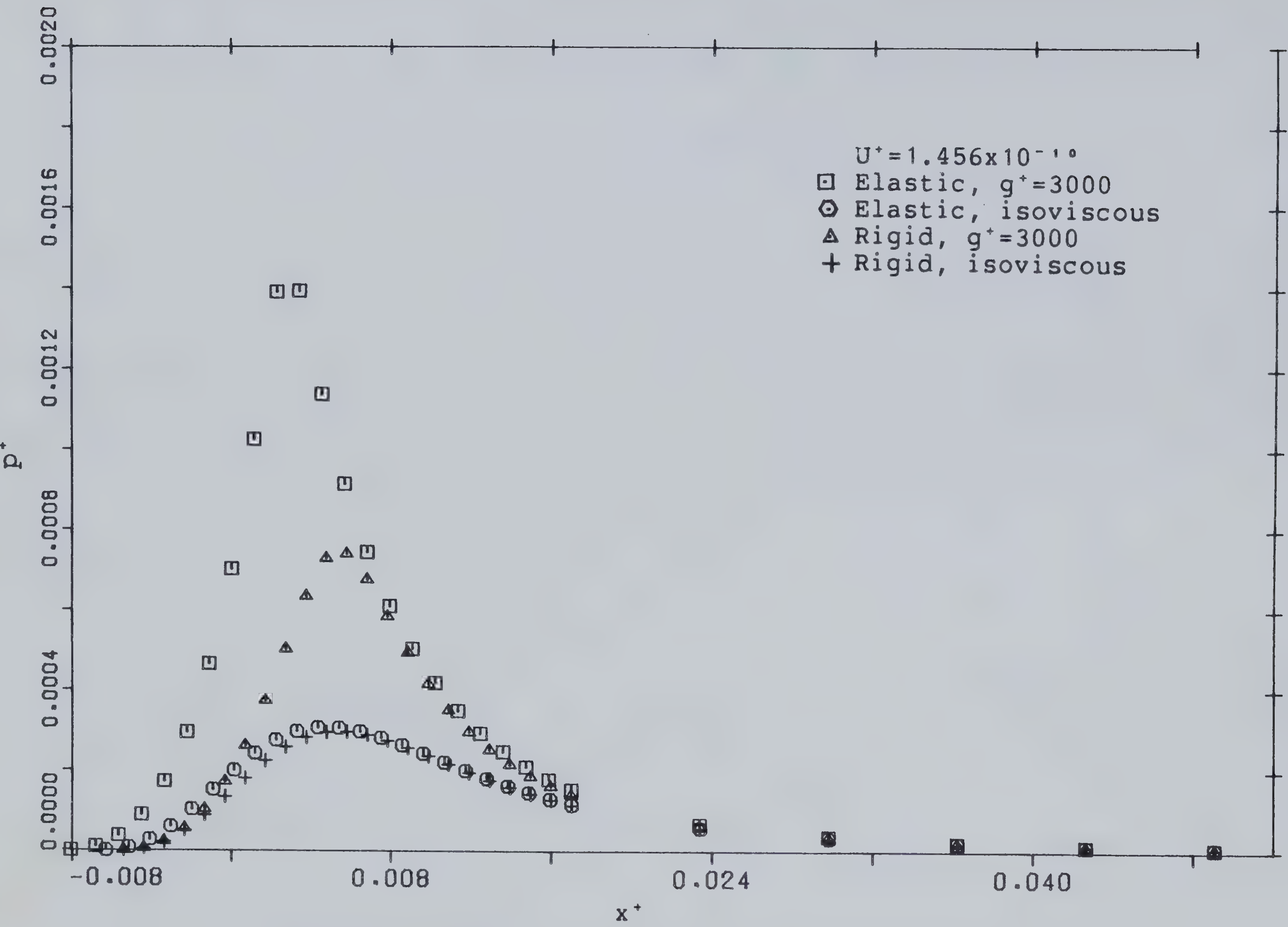

Fig(26) Pressure distributions for $h^+_{min}=0.65\times10^{-4}$

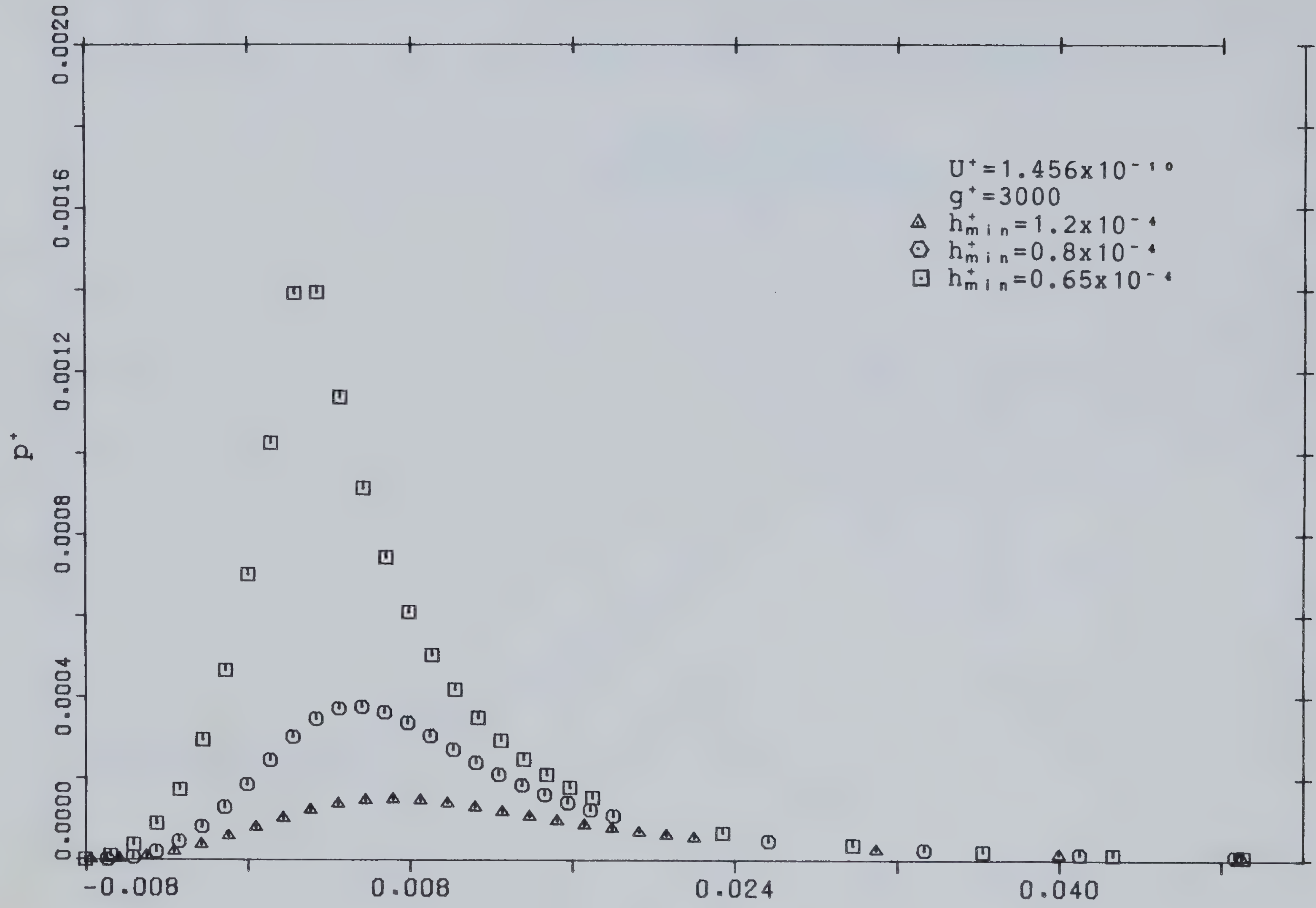

Fig(27) Pressure distributions for various h^+_{min}'s for elastic cylinder

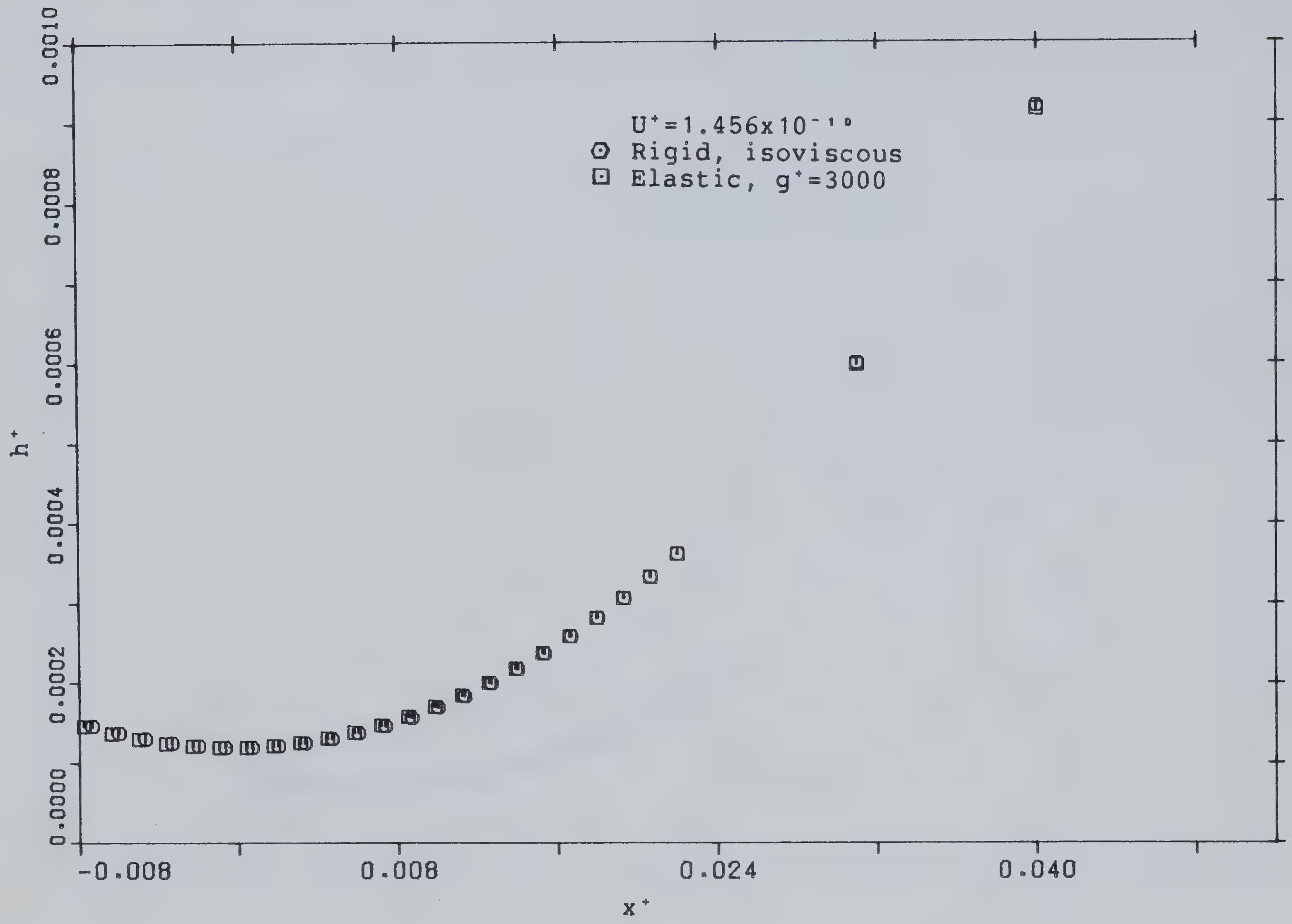

Fig(28) Film thickness variation for $h^+_{min}=1.2\times10^{-4}$

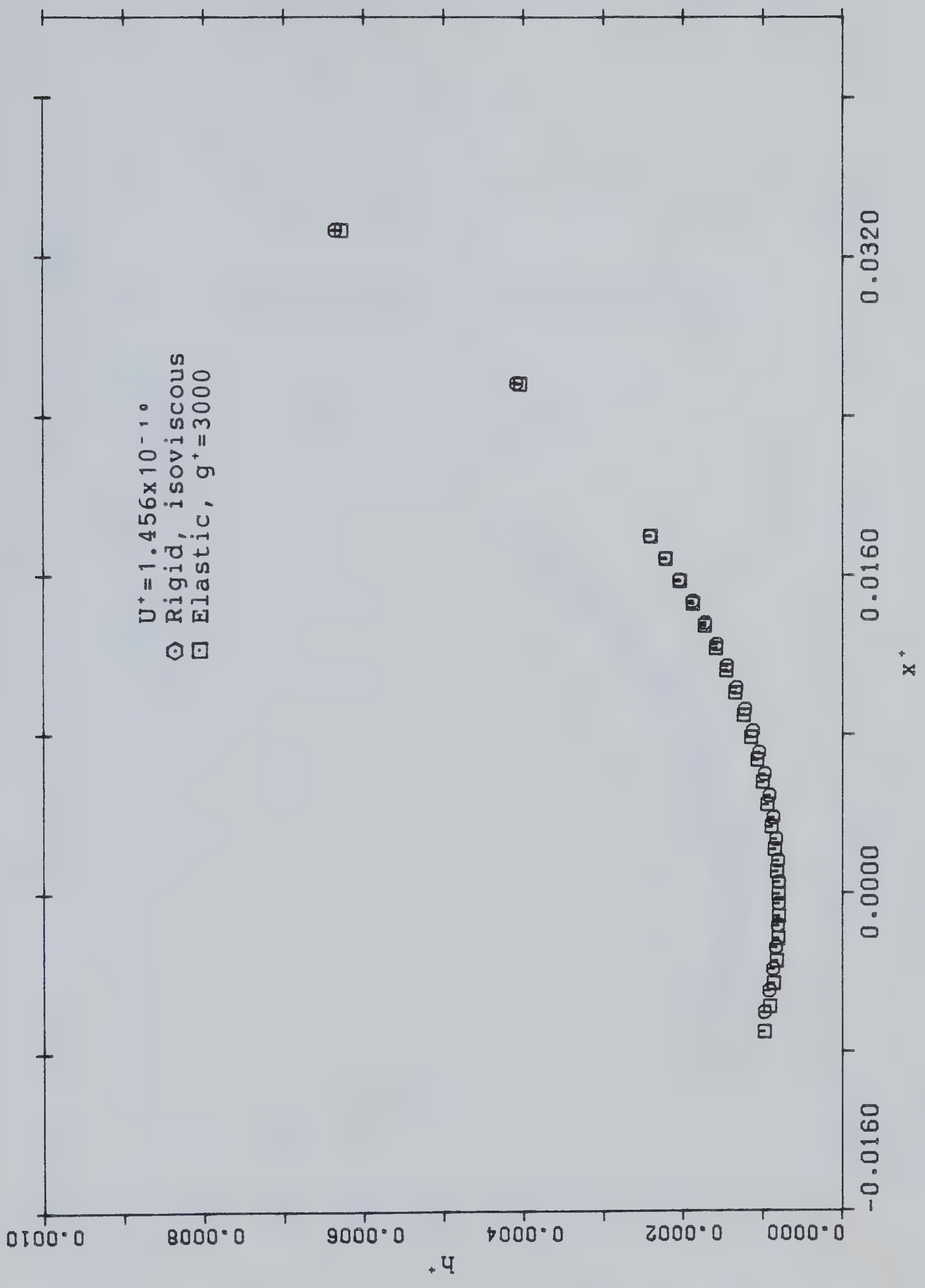

Fig(29) Film thickness variation for $h^+_{min}=0.8x10^{-4}$

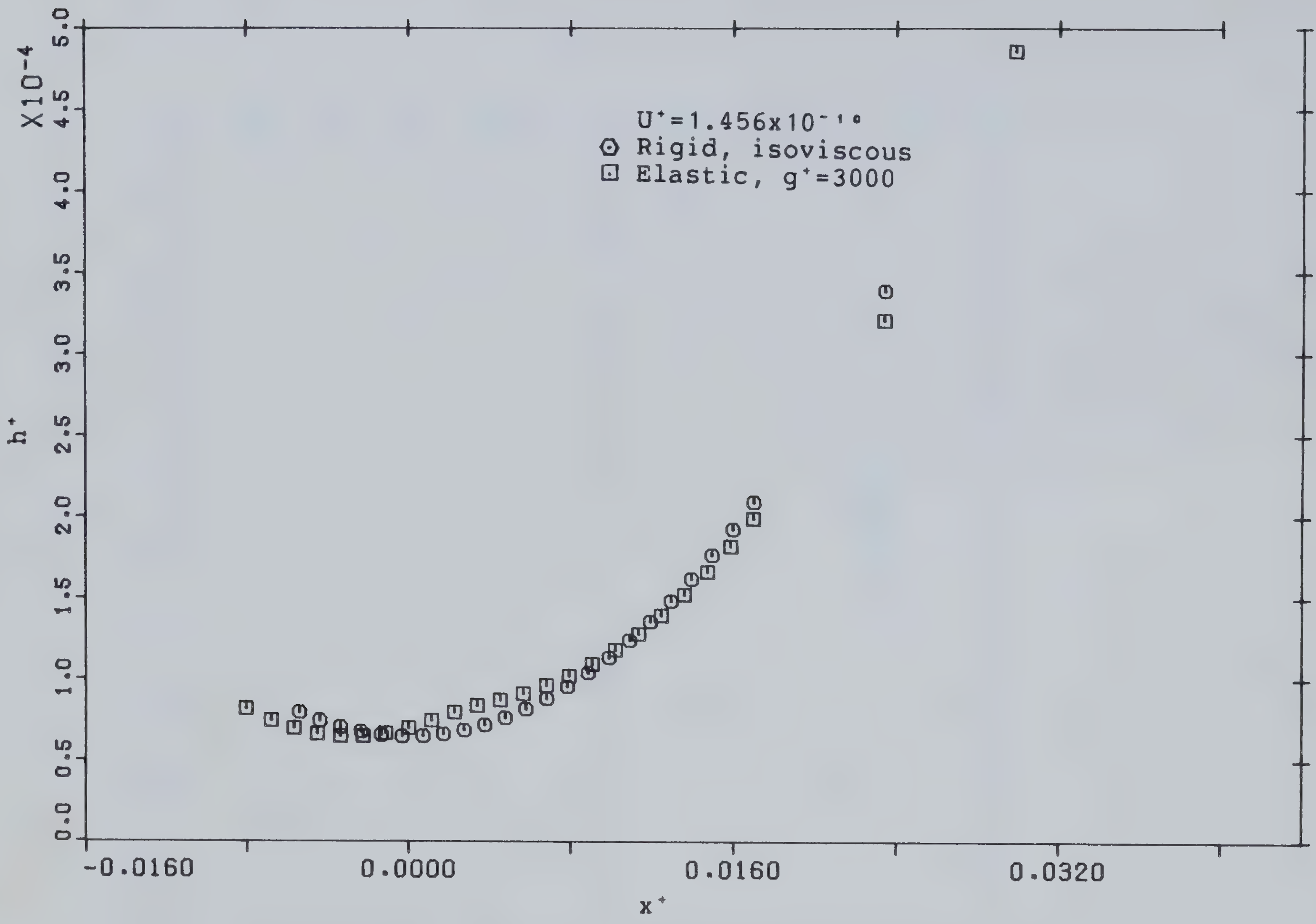

Fig(30) Film thickness variation for $h^+_{min}=0.65\times10^{-4}$

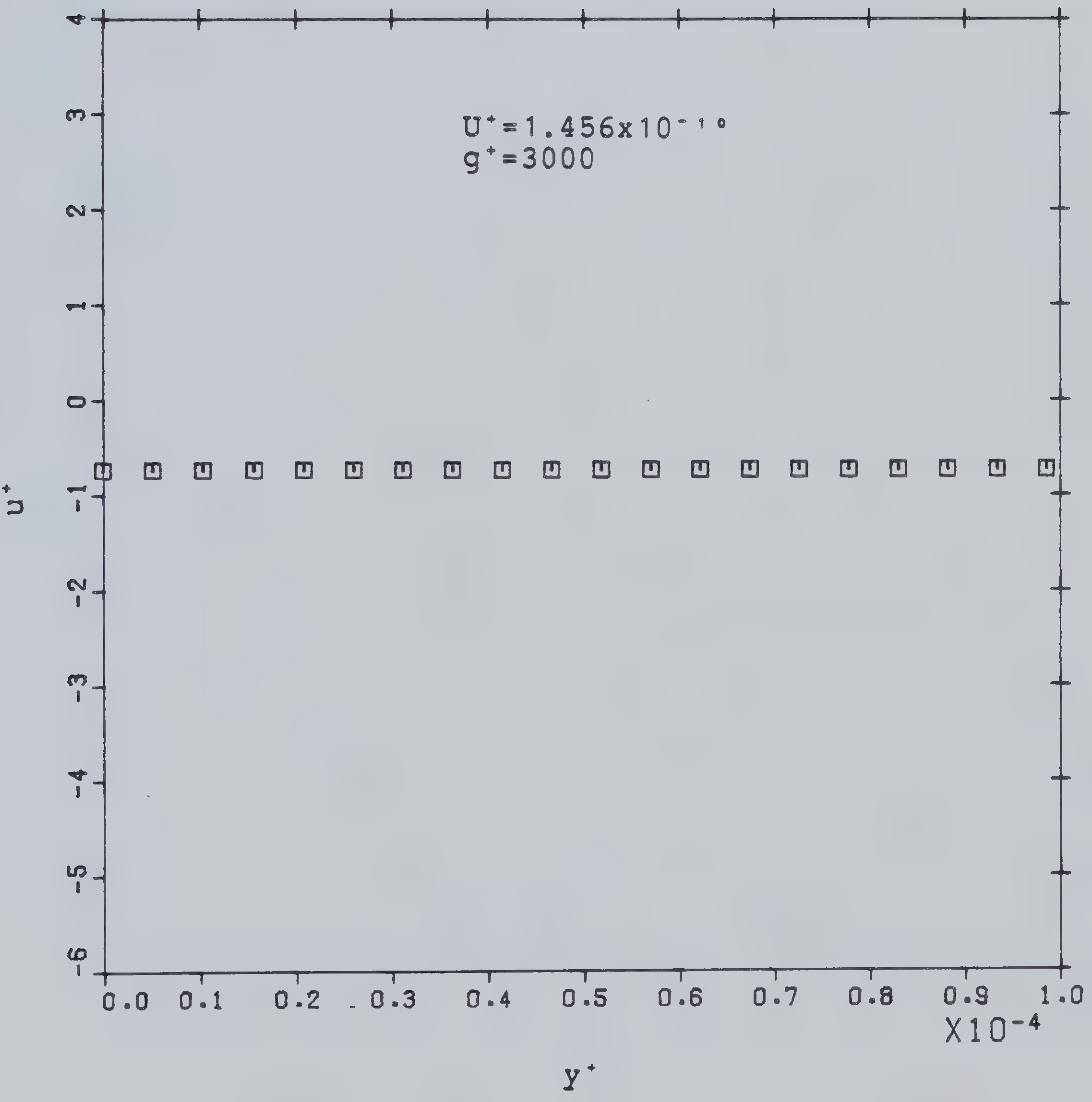

Fig(31) Velocity distribution at outlet for $h^+_{min}=0.8\times10^{-4}$ for elastic cylinder

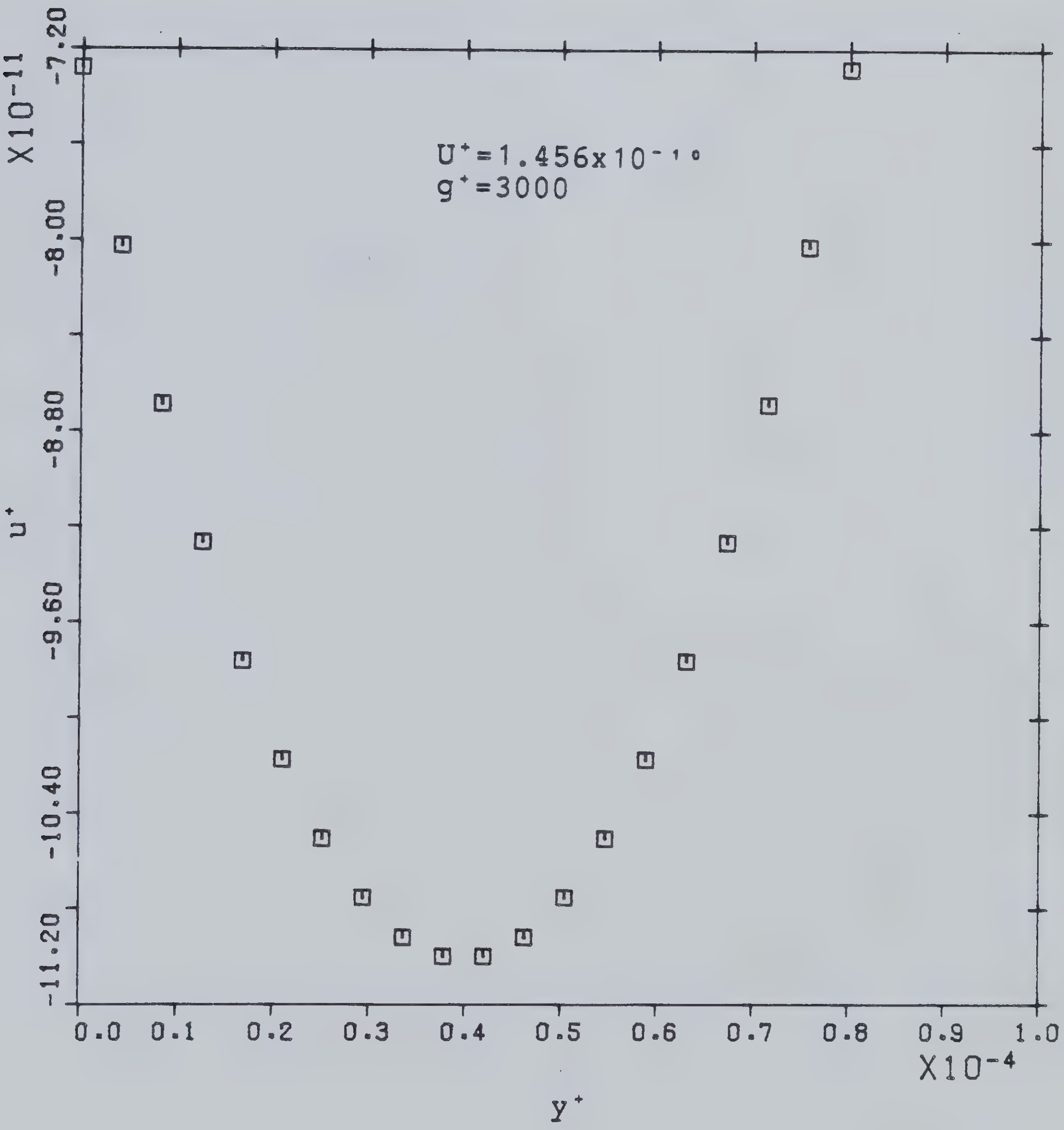

Fig(32) Velocity distribution at which h is minimum for $h^+_{min}=0.8\times10^{-4}$ for elastic cylinder

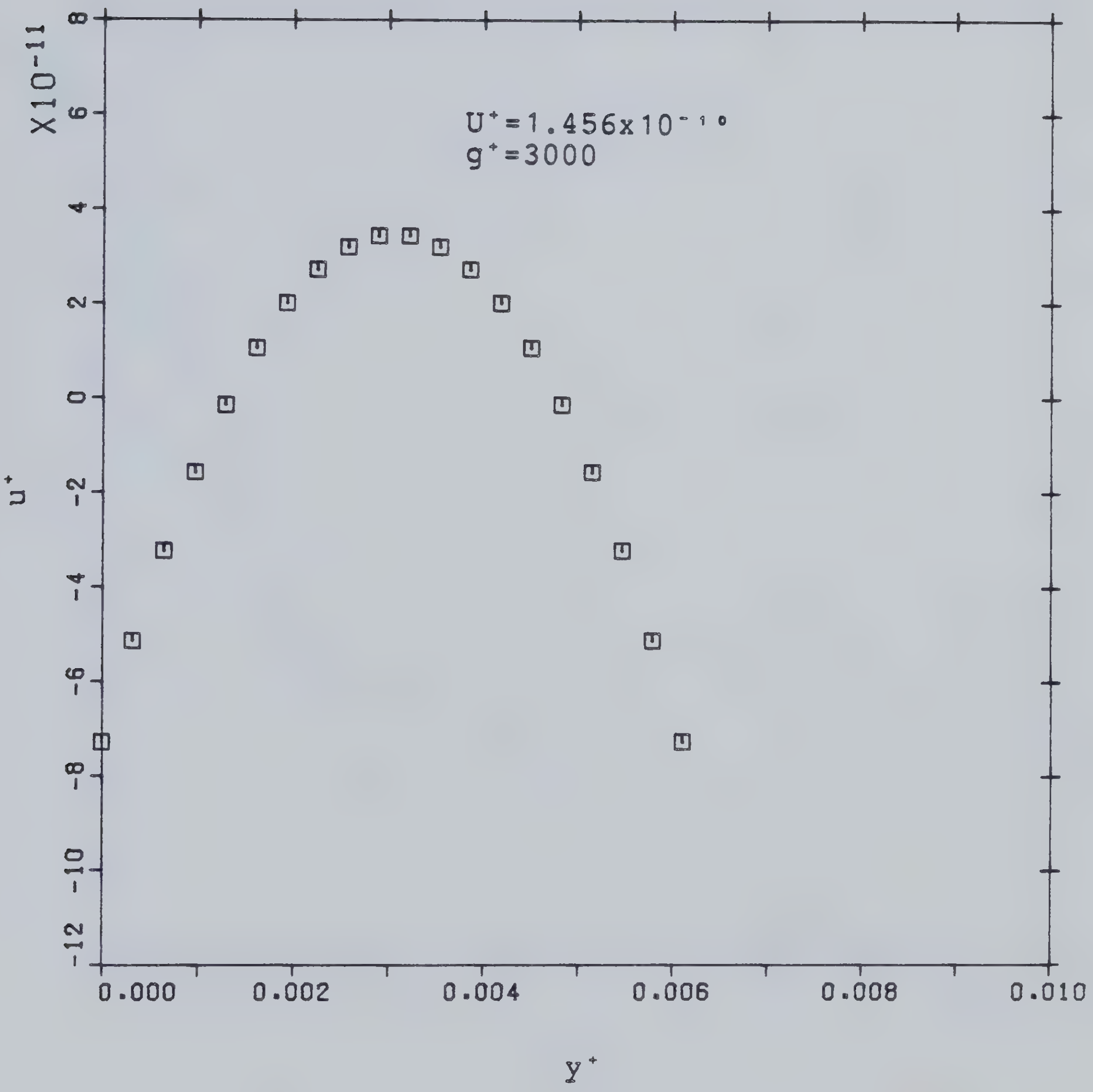

Fig(33) Velocity distribution at inlet for $h^{+}_{min}=0.8\times10^{-4}$ for elastic cylinder

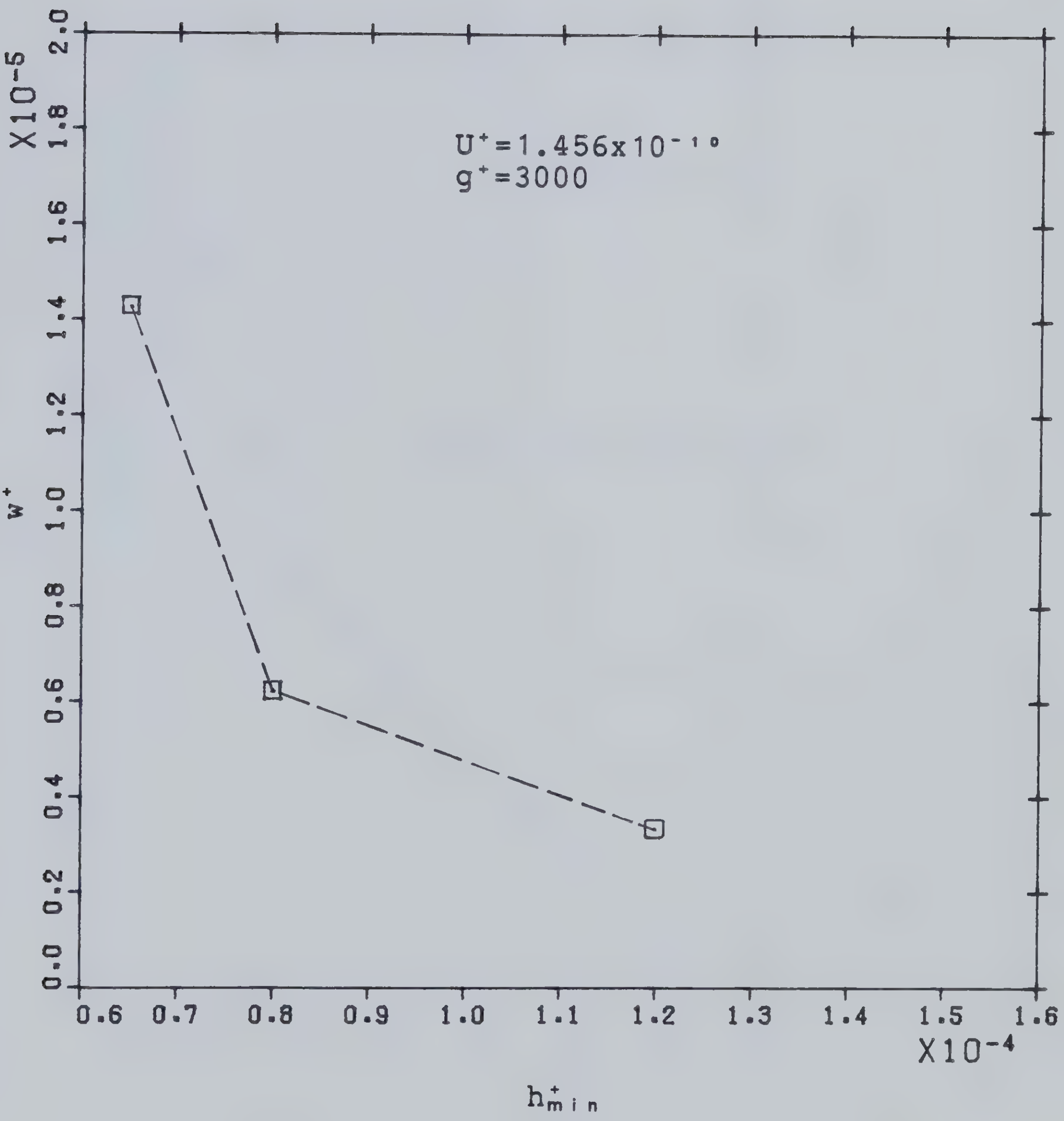

Fig(34) Variation of load with minimum film thickness for elastic cylinder

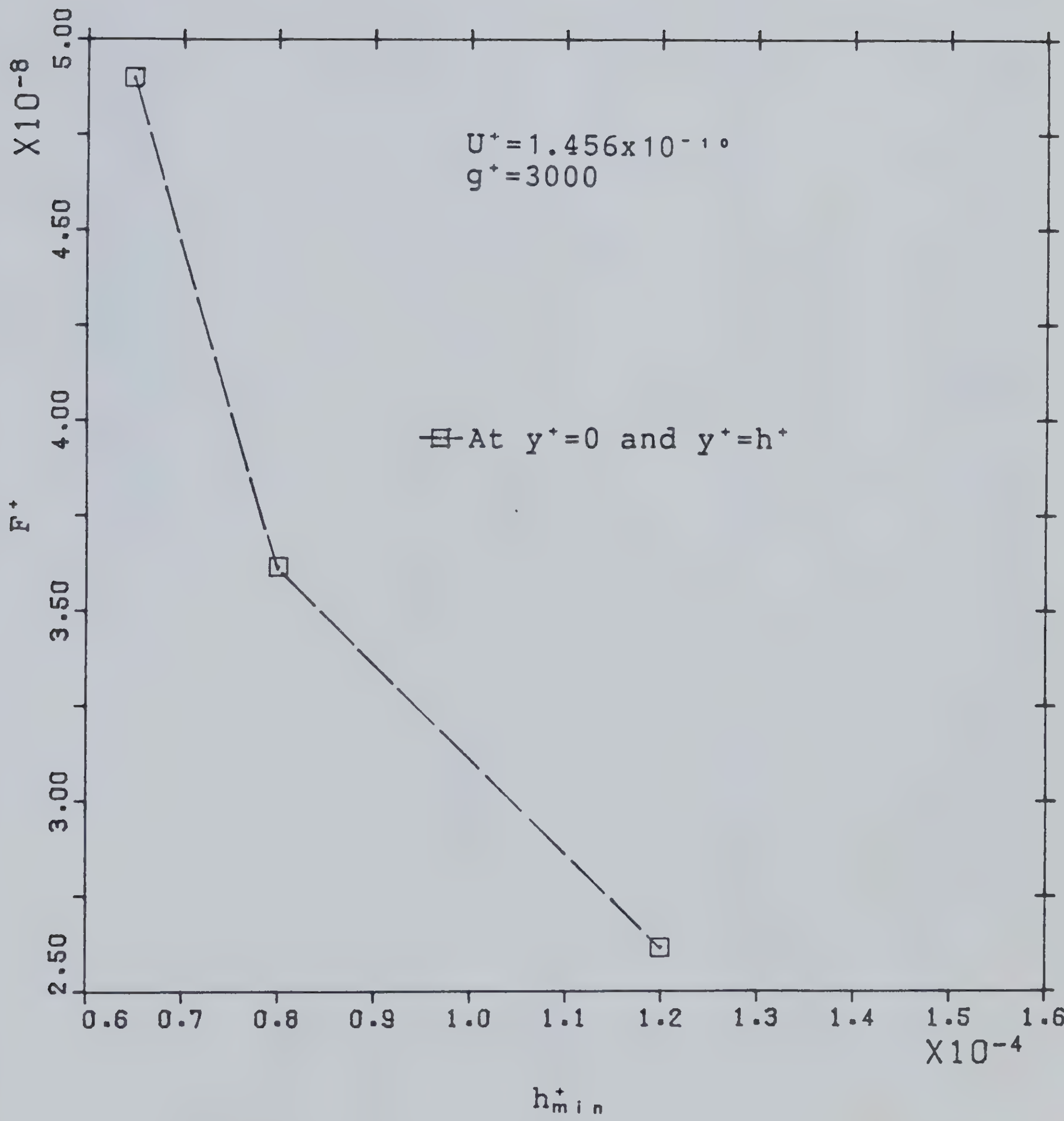

Fig(35) Variation of drag with minimum film thickness for elastic cylinder

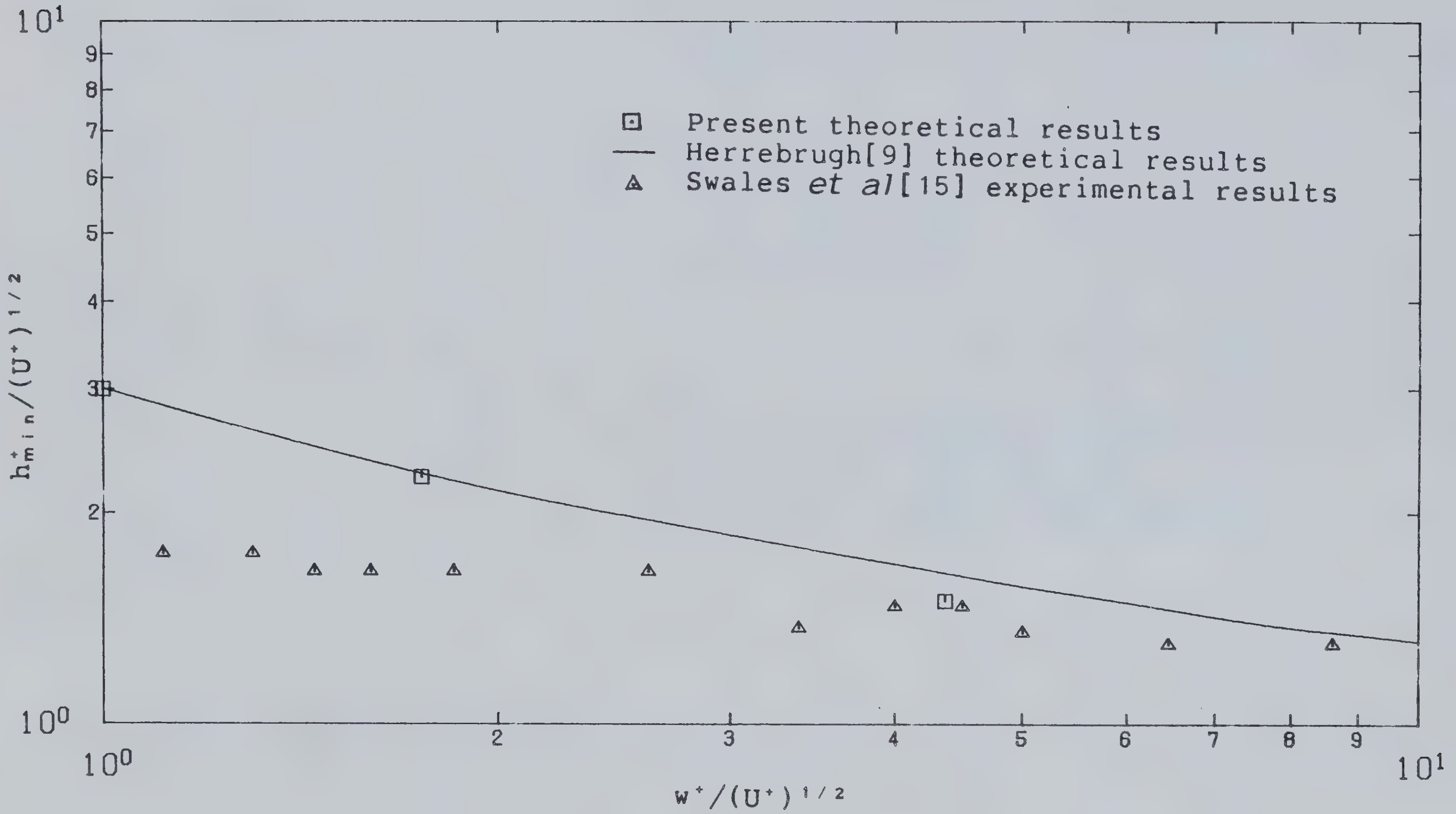

Fig(36)Comparison of present theoretical results with earlier experimental and theoretical results for g^+=0.933

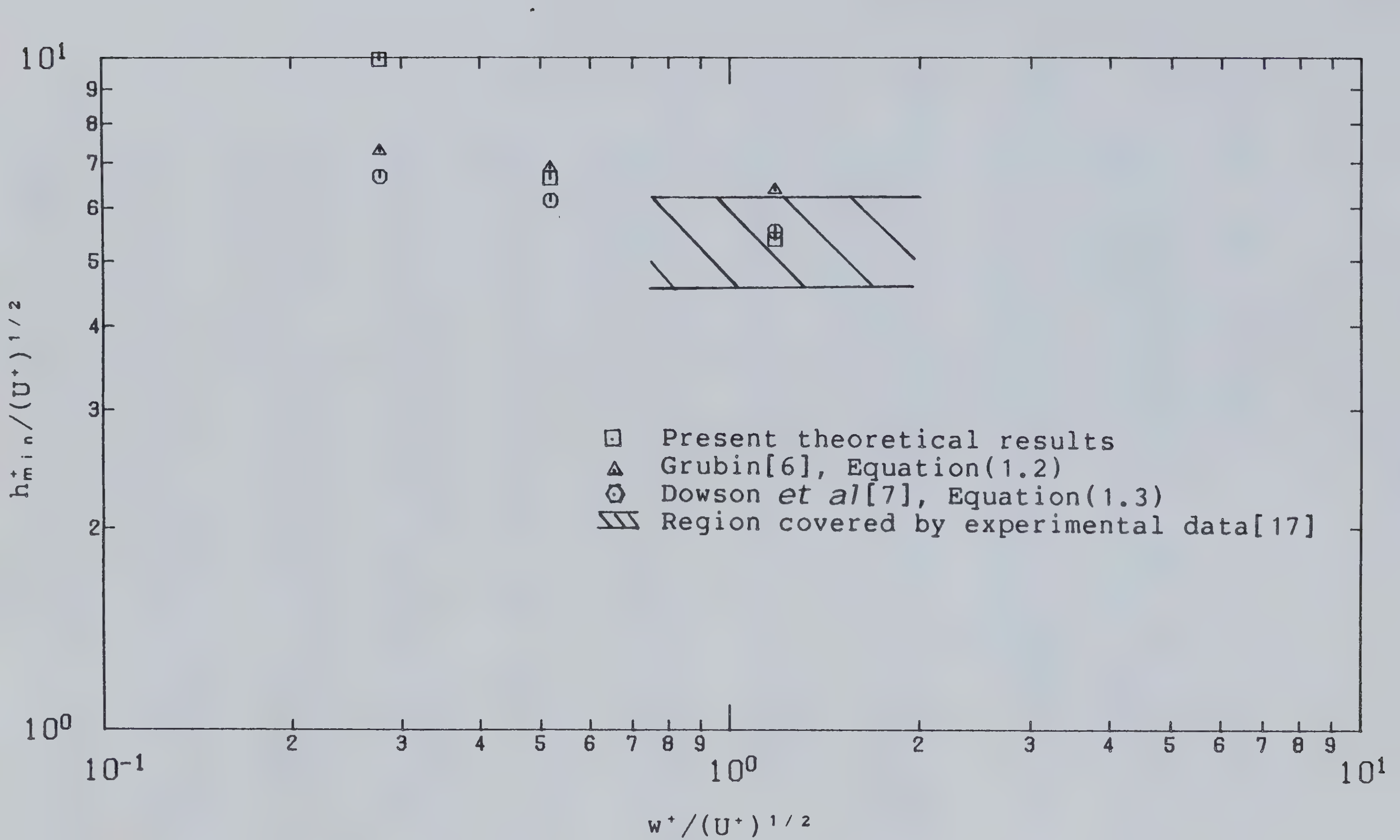

Fig(37)Comparison of present theoretical results with earlier experimental and theoretical results for $g^+=3000$

REFERENCES

1. Martin, H.M., Lubrication of gear teeth, Engineering, **102**, 119-121, 1916.

2. Crook, A.W., Simulated gear-tooth contact: some experiments upon their lubrication and sub-surface deformations, Proc. Inst. Mech. Engrs. London. **171**, 187, 1957.

3. Peppler, W., Druckubertragung an geschmierten zylindrischen Gleitund Walzflachen, V.D.I.-Forschungsheft, 391, 1938.

4. Meldahl, A., Contribution to the theory of the lubrication of gears and of the stressing of the lubricated flanks of gear teeth, Brown Boveri Review, **28**, No. 11, 374, 1941.

5. Gatcombe, E.K., Lubrication characteristics of involute spur-gears—a theoretical investigation, Trans. Amer. Soc. Mech. Engrs., **67**, 177, 1945.

6. Grubin, A.N. and Vinogradova, I.E., Central Scientific Research Institute for Technology and Mechanical Engineering, Book No.30, Moscow, D.S.I.R. Translation No.337, 1949.

7. Dowson, D. and Whitaker, A.V., The Isothermal Lubrication of Cylinders, ASLE Tran., 8, 224-234, 1965.

8. Osterle, J.F. and Stephenson, R.R., A direct solution of the elastohydrodynamic lubrication problem, Trans. Amer. Soc. Lub. Engrs., **5**, No.2, 365, 1962.

9. Herrebrugh, K., Solving the incompressible and isothermal problem in elastohydrodynamic lubrication through an integral equation, Tran. ASME F90, 262-270, 1968.

10. Cheng, H.S., Isothermal elastohydrodynamic theory for the full range of pressure-viscosity coefficient, Tran. ASME F94, 35-43, 1972.

11. Roberts, A.D. and Tabor, D., Fluid film lubrication of rubber—an interferometric study, Wear **11**, 163, 1968.

12. Higginson, G.R., A model experiment in elastohydrodynamic lubrication, Int. F. Mech. Sci., **4**, 205, 1962.

13. Roberts, A.D. and Swales, P.D., The elastohydrodynamic lubrication of a highly elastic cylindrical surface, Br. F. Appl. Phys. (F. Phys. D), Series 2, **2**, 1317, 1969.

14. Baglin, K.P. and Archard, J.F., An analytical solution of the elastohydrodynamic lubrication of materials of low elastic modulus, Proc. Inst. Mech. Engrs., Symposium on Elastohydrodynamic Lubrication, 13-21, 1972.

15. Swales, P.D., Dowson, D. and Latham, J.L., Theoretical and experimental observations of the behavior of soft elastic materials under elastohydrodynamic conditions, Proc. Inst. Mech. Engrs., Symposium on Elastohydrodynamic Lubrication, 22-28, 1972.

16. Cameron, A., Principal of lubrication, Longmans, 187-212, 1966.

17. Crook, A.W., The lubrication of rollers, II, Film thickness with relation to viscosity and speed, Phil. Trans. **A254**, 223, 1961.

BIBLIOGRAPHY

Rodkiewicz, C.M. and Srinivasan, V., Elastohydrodynamic lubrication in rolling and sliding contacts, Trans. ASME F94, 324-329, 1972.

Dowson, D. and Higginson, G.R., Elasto-hydrodynamic Lubrication, 1st Edition, Pergamon, 1977.

Higginson, G.R., Progress in elastohydrodynamic, Elastohydrodynamics and related topics, London, 3-12, 1979.

Schlichting, H., Boundary Layer Theory, McGraw-Hill, New York, 1979.

APPENDIX I

Input data

Radius of cylinder (R_2)	0.0635 m
Material of cylinder	rubber
Atmospheric absolute viscosity (μ_0)	0.138 Ns/m^2
Modulus of elasticity (E_2)	24×10^6 N/m^2
Poisson's ratio (υ_2)	0.5
Cylinder rotating speed (u_2)	0
Slider speed (u_1)	0.59 m/s - 2.37 m/s
Load (w)	525 N/m - 57800 N/m

APPENDIX II

Input data for soft material

Radius of cylinder (R_2)	0.0635 m
Material of cylinder	rubber
Atmospheric absolute viscosity (μ_0)	0.138 Ns/m^2
Modulus of elasticity (E_2)	24x10^6 N/m^2
Poisson's ratio (ν_2)	0.5
Cylinder rotating speed (u_2)	0
Slider speed (u_1)	1.185 m/s
Pressure viscosity exponent (α)	1.45x10^{-8} m^2/N
Minimum film thickness (h_{min})	1.905x10^{-2} mm to 3.81x10^{-2} mm

Input data for hard material

Radius of cylinders (R_1, R_2)	0.0508 m
Material of cylinders	steel
Atmospheric absolute viscosity (μ_0)	0.138 Ns/m^2
Modulus of elasticity (E_1, E_2)	20.7×10^{10} N/m^2
Poisson's ratio (υ_1,υ_2)	0.3
Cylinder rotating speeds (u_1, u_2)	3.048 m/s
Pressure viscosity exponent (α)	1.32×10^{-8} m^2/N
Minimum film thickness (h_{min})	1.651×10^{-3} mm to 3.048×10^{-3} mm